



HAL
open science

Mineralogy of a Possible Ancient Lakeshore in the Sutton Island Member of Mt. Sharp, Gale Crater, Mars, From Mastcam Multispectral Images

James T Haber, Briony Horgan, Abigail A Fraeman, Jeffrey R Johnson, Jim F Bell, Melissa S Rice, Christina Seeger, Nicolas Mangold, Lucy Thompson, Danika Wellington, et al.

► To cite this version:

James T Haber, Briony Horgan, Abigail A Fraeman, Jeffrey R Johnson, Jim F Bell, et al.. Mineralogy of a Possible Ancient Lakeshore in the Sutton Island Member of Mt. Sharp, Gale Crater, Mars, From Mastcam Multispectral Images. *Journal of Geophysical Research. Planets*, 2022, 127 (10), pp.e2022JE007357. 10.1029/2022je007357 . hal-04665760

HAL Id: hal-04665760

<https://hal.science/hal-04665760v1>

Submitted on 31 Jul 2024

HAL is a multi-disciplinary open access archive for the deposit and dissemination of scientific research documents, whether they are published or not. The documents may come from teaching and research institutions in France or abroad, or from public or private research centers.

L'archive ouverte pluridisciplinaire **HAL**, est destinée au dépôt et à la diffusion de documents scientifiques de niveau recherche, publiés ou non, émanant des établissements d'enseignement et de recherche français ou étrangers, des laboratoires publics ou privés.

Mineralogy of a Possible Ancient Lakeshore in the Sutton Island Member of Mt. Sharp, Gale Crater, Mars, From Mastcam Multispectral Images



Key Points:

- Mastcam multispectral data in Sutton Island exhibit bands >900 nm consistent with Fe/Mg-clay minerals like nontronite
- Sutton Island was deposited in a lowstand/nearshore environment and exposed to more subaerial weathering than the nearby Murray
- The presence of abundant clay minerals in Sutton Island significantly reduced fluid flow and alteration during later diagenesis

Supporting Information:

Supporting Information may be found in the online version of this article.

Correspondence to:

J. T. Haber,
haberj@purdue.edu

Citation:

Haber, J. T., Horgan, B., Fraeman, A. A., Johnson, J. R., Bell, J. F. III., Rice, M. S., et al. (2022). Mineralogy of a possible ancient lakeshore in the Sutton Island member of Mt. Sharp, Gale crater, Mars, from Mastcam multispectral images. *Journal of Geophysical Research: Planets*, 127, e2022JE007357. <https://doi.org/10.1029/2022JE007357>




Received 5 MAY 2022
Accepted 21 SEP 2022

Author Contributions:

Conceptualization: Briony Horgan
Data curation: Briony Horgan
Formal analysis: Briony Horgan
Funding acquisition: Briony Horgan
Investigation: Briony Horgan
Methodology: Briony Horgan
Project Administration: Briony Horgan
Resources: Briony Horgan
Software: Briony Horgan
Supervision: Briony Horgan
Validation: Briony Horgan
Visualization: Briony Horgan

© 2022 The Authors.

This is an open access article under the terms of the [Creative Commons Attribution-NonCommercial License](https://creativecommons.org/licenses/by-nc/4.0/), which permits use, distribution and reproduction in any medium, provided the original work is properly cited and is not used for commercial purposes.

James T. Haber¹ , Briony Horgan¹ , Abigail A. Fraeman² , Jeffrey R. Johnson³ , Jim F. Bell III⁴ , Melissa S. Rice⁵, Christina Seeger⁶, Nicolas Mangold⁷ , Lucy Thompson⁸ , Danika Wellington⁹, Ed Cloutis¹⁰ , and Samantha Jacob⁴ 

¹Department of Earth, Atmospheric and Planetary Sciences, Purdue University, West Lafayette, IN, USA, ²Jet Propulsion Laboratory, California Institute of Technology, Pasadena, CA, USA, ³Johns Hopkins University Applied Physics Laboratory, Laurel, MD, USA, ⁴School of Earth and Space Exploration, Arizona State University, Tempe, AZ, USA, ⁵Department of Geology, Western Washington University, Bellingham, WA, USA, ⁶Division of Geologic and Planetary Sciences, California Institute of Technology, Pasadena, CA, USA, ⁷Laboratoire de Planétologie et Géodynamique, Université Nantes, Nantes Cedex, France, ⁸Planetary and Space Science Centre, University of New Brunswick, Fredericton, NB, USA, ⁹KBR, Inc, Houston, TX, USA, ¹⁰Department of Geography, University of Winnipeg, Winnipeg, MB, USA

Abstract The *Curiosity* rover on the Mars Science Laboratory mission has found extensive evidence that Gale crater once hosted a habitable lacustrine environment; however, there are remaining questions about the chemistry and duration of the lake and the nature of the climate at the time. In this study, we use Mastcam multispectral data to investigate the mineralogy of the Sutton Island member of the Murray formation, a part of the basal layers of Mt. Sharp, which consists of heterolithic mudstone and sandstone that are distinct from the finely laminated mudstones that dominate much of the Murray. Sutton Island includes at least one instance of desiccation cracks, indicative of subaerial exposure, and uniquely irregular diagenetic features that may be related to local bedrock permeability. These features suggest that Sutton Island experienced a complex history of deposition and diagenesis which may be crucial for understanding changing water-rock interactions within Gale. We find that most Mastcam bedrock spectra in this region lack the absorptions associated with hematite found throughout the Murray, and instead show deeper absorptions shifted toward longer wavelengths that are more consistent with Fe-smectites such as nontronite. Elemental chemistry from ChemCam supports this interpretation, as SiO, MgO, Li, and the chemical index of alteration are elevated in this region. Combined with observations of bedrock sedimentology, this suggests that Sutton Island was deposited in a nearshore or low stand environment, and we hypothesize that the clay minerals were produced in this region due to sub-aerial exposure and weathering in a semi-arid climate.

Plain Language Summary The *Curiosity* rover on the Mars Science Laboratory mission has found extensive evidence that Gale crater once hosted a habitable lake environment; however, there are remaining questions about the chemistry and timing of the lake and the nature of the climate at the time. In this study, we use Mastcam data to investigate the composition of the Sutton Island member of the Murray formation, which consists of mixed fine and coarse grained rocks that are distinct from the very fine-grained rocks that dominate much of the Murray. Sutton Island includes mudcracks, indicative of surface exposure, and irregular alteration features that may be related to local bedrock differences. These features suggest that Sutton Island experienced a complex history of deposition and alteration which may be crucial for understanding changing water-rock interactions within Gale. We find that most bedrock in this region lack features associated with hematite found throughout the Murray, and instead show features that are more consistent with clay minerals. Combined with observations of mudcracks and chemistry data, this suggests that Sutton Island was deposited in a nearshore environment, and we hypothesize that the clays were produced in this region due to surface exposure and weathering in a semi-arid climate.

1. Introduction

The findings of NASA's *Curiosity* rover on the Mars Science Laboratory (MSL) mission provide extensive evidence that Gale crater once hosted a habitable lacustrine environment. *Curiosity* has found chemical, mineralogical, and sedimentological evidence for a long-lived lake of liquid water that contained organic molecules

Writing – original draft: Briony Horgan
Writing – review & editing: Briony Horgan

and other critical elements for life (Grotzinger et al., 2014). However, the chemistry of this lake environment is not fully constrained because of the complicated history of water interactions experienced by the sediments both during and long after deposition. In particular, it is unclear which secondary minerals in Gale's rock record formed in primary lacustrine (Bristow et al., 2018; Hurowitz et al., 2017; Rapin et al., 2019) versus later diagenetic events (Fraeman, Edgar, et al., 2020; Fraeman, Johnson, et al., 2020; Horgan et al., 2020; Rampe et al., 2017). Understanding the origin of secondary minerals is crucial for studying habitability in Gale because these minerals provide key constraints on the timing and types of environments that existed and the preservation of biosignatures and organics.

Curiosity has been exploring Gale crater since 2012 and has traversed over 500 m of stratigraphy of the central crater mound Aeolis Mons, informally called Mt. Sharp. Rocks that form the base of Mt. Sharp are members of the Murray formation, which is dominated by lacustrine mudstones featuring early and late diagenetic textures (Grotzinger et al., 2014). In this work we focus on the Sutton Island (SI; Figure 1) member of the Murray formation, a heterolithic mudstone and sandstone member. This sedimentology is distinct from the rest of the Murray, which otherwise exhibits clear member boundaries between laminated lacustrine mudstones and fluvial sandstones (Fedo et al., 2018; Siebach et al., 2019). Sutton Island also contains the only example so far of filled fractures resembling desiccation cracks, indicative of surface exposure (Stein et al., 2018). We hypothesize that Sutton Island sediments may have been deposited closer to shore or at periods of low lake levels and thus the chemistry and mineralogy of SI may provide a different constraint on lake chemistry and paleoclimate than the rest of the Murray. However, in-situ mineralogy from drilled samples is limited in this region; we aim to solve this using Mastcam multispectral data to constrain variations in the iron bearing mineralogy that may be due to changes in lake chemistry and paleoclimate.

Additionally, several different diagenetic features are more common in Sutton Island than neighboring members, including large dark fracture fills, concretions of flat, round and irregular morphologies, dark mottled bedrock, and bedrock with meter-scale color variability from red to tan or gray (Sun et al., 2019). However, the timing of the diagenetic events, how these diagenetic events may have affected the mineralogy of SI, and why SI experienced a diagenetic history that is distinct from the rest of the Murray are all not well understood.

These observations suggest that the mineralogy of SI may provide important constraints on the history of aqueous activity and environmental conditions in Gale crater. However, little bulk mineralogy data is available for Sutton Island or the overlying member Blunts Point because of a dearth of drilled samples within this region due to a failure of the *Curiosity* drill feed mechanism around that time.

In this study we use Mastcam visible/near-infrared (445–1,012 nm) multispectral data to better constrain the mineralogy of Sutton Island. We analyze Mastcam relative reflectance spectra from bedrock targets and diagenetic features throughout the Sutton Island and neighboring members and compare trends in Mastcam spectral data to data collected by ChemCam and APXS to constrain the mineralogy of Fe-bearing alteration phases, including Fe-bearing oxides, sulfates, and phyllosilicates. We use decorrelation stretches to look at variability within Mastcam images of individual bedrock targets, and we compare Mastcam spectra to lab spectra to constrain their mineralogy and help us better understand the depositional and alteration history of the Murray formation.

2. Background

2.1. Sedimentology and Stratigraphy

The Sutton Island member of the Murray formation is a heterolithic mudstone and sandstone that makes up ~98 m of the section of Mt. Sharp investigated to date by MSL, from approximately –4,375 to –4,280 m, and approximately mission sol 1,469 to sol 1,696 (Siebach et al., 2019). The heterolithic facies in SI are distinct from the rest of the Murray, which otherwise exhibits clear member boundaries between laminated lacustrine mudstones and fluvial sandstones (Fedo et al., 2018; Rivera-Hernandez et al., 2020). The heterolithic facies has been interpreted as potentially indicating a mixture of fluvial and lacustrine deposition within a marginal lake setting, which is consistent with evidence for sub-aerial exposure from mudcracks indicative of desiccation under at least transient low lake levels (Stein et al., 2018). The color of SI bedrock ranges from reddish-brown to a deeper dark red depending on illumination conditions. Additionally, bedrock color can be observed transitioning from tan to brown to red within some outcrops (Section 4.1). This contrasts from the adjacent members of the

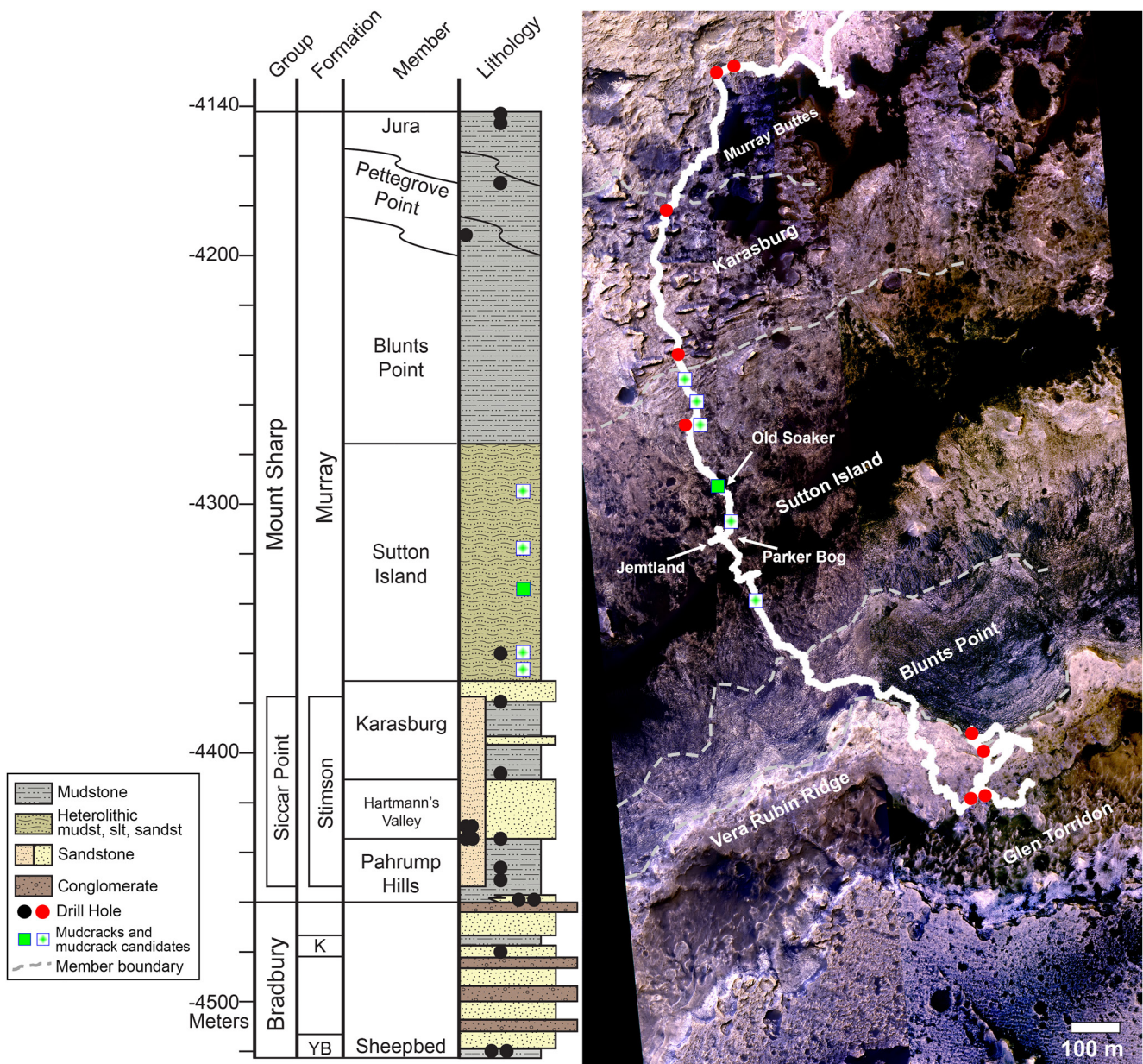


Figure 1. Stratigraphic column (left; modified from Fedo et al., 2019) and HiRISE enhanced color image (right; ESP_021610_1755, ESP_035772_1755; NASA/JPL/UAirizona) overlain with the *Curiosity* rover traverse showing members of the Murray formation along with the locations of drill holes, desiccation cracks, and arrows pointing to key outcrops.

Murray formation where facies are mostly homogenous lacustrine mudstone with a brown-red color (Figure S1 in Supporting Information S1).

Stratigraphically below the Sutton Island member, the Murray formation is dominated by mudstones and some sandstones, consistent with deposition in fluvial and lacustrine environments. The basal member of the Murray formation, Pahrump Hills, is ~14 m thick and contains mostly mudstone with some cross-stratified sandstone, consistent with deposition in a fluvio-deltaic environment (Fedo et al., 2018). This is overlain by the ~25 m thick Hartmann's Valley member, which contains sedimentary rocks of varying grain sizes from silt to sand as well as evidence of meter-scale cross-stratification, suggesting a fluvial or possibly aeolian depositional environment (Gwizd et al., 2019). The subsequent Karasburg member consists of mudstone and sandstone facies at distinct intervals (Fedo et al., 2018). The upper Pahrump Hills and Karasburg members are unconformably overlain by

the aeolian sandstones of the Stimson Formation (Banham et al., 2018), which most notably occurs as caprocks on buttes and mesas in this area.

Above Sutton Island, the Murray formation transitions into Vera Rubin ridge (VRR), a linear topographic feature interpreted to be diagenetic in origin (Fraeman, Edgar, et al., 2020; Fraeman, Johnson, et al., 2020). The Blunts Point member forms the northern slope of Vera Rubin ridge, and contains fine grained laminated mudstone with sparse cross-stratified sandstone and many Ca-sulfate veins and lighter toned bedrock. These facies suggest deposition out of suspension in a stable lacustrine environment (Edgar et al., 2020; Fedo et al., 2018). The transition in facies in the Murray from Pahrump Hills through Blunts Point is generally consistent with progradation of fluvial to lacustrine deposition, possibly with multiple episodes of deposition (Fedo et al., 2018; Grotzinger et al., 2015; Rivera-Hernandez et al., 2020).

2.2. Mineralogy

Mineralogy of the Murray formation has been primarily determined using the Chemistry and Mineralogy (CheMin) X-ray diffractometer, which has collected data on the bulk mineralogy of the crystalline fraction of powdered drill samples at 19 locations along the rover traverse as of sol 2,300 in January 2019 (Blake et al., 2012; Rampe et al., 2020). The mineralogy of the Murray formation includes a mixture of crystalline igneous (olivine, pyroxene, feldspar) and secondary (phyllosilicates, sulfates, oxides, etc.) minerals directly identified by CheMin, as well as a significant X-ray amorphous component with variable abundances (15%–73%; Rampe et al., 2020) and compositions (e.g., Fe-rich to Si-rich; Smith et al., 2021). The CheMin detections are consistent with mineralogy of the region below VRR inferred from orbital visible/near-infrared (VNIR; 0.3–2.5 μm) spectra, which include patchy detections of Fe/Mg-smectite, hydrated silica, sulfates, and hematite (Bristow et al., 2018; Fraeman et al., 2016; Milliken et al., 2010).

Phyllosilicate minerals have been found in almost every sample deposited in a fluvio-lacustrine environment that has been analyzed by the CheMin instrument on Curiosity, but the composition of these clay minerals changed as the rover moved up section, from trioctahedral Fe-smectite (e.g., Fe-bearing saponite) in Yellowknife Bay to mixtures with dioctahedral smectites (e.g., montmorillonite) in the Murray (Bristow et al., 2018; Rampe et al., 2020). Within the Murray, the ratio of dioctahedral to trioctahedral smectites collected by the drill sampling system increased upsection within the Karasburg member from 1:1 for Marimba to 2:1 for Quela, which was comparable to 5:3 for Sebina at the base of the SI member. On Earth, dioctahedral smectites commonly form due to sub-aerial weathering (Catalano, 2013; Chamley, 1989; Chemtob et al., 2017). The transition from trioctahedral to dioctahedral smectite has been interpreted to suggest a change in the aqueous alteration environment to a more open-system (Bristow et al., 2018).

Hematite dominates Mastcam multispectral observations of most Murray formation bedrock targets, which exhibit weak to moderate absorptions at 867 nm consistent with crystalline fine-grained hematite (Fraeman, Edgar, et al., 2020; Fraeman, Johnson, et al., 2020; Jacob et al., 2020; Wellington et al., 2017). Drill samples in the lower Murray through VRR all contained varying amounts of hematite (3–15 wt.%; Rampe et al., 2020). CheMin XRD analysis of the crystalline phases in Sebina, the only drill location in Sutton Island and located at its very base, indicated that it contained 6.9 ± 0.2 wt.% hematite along with 19 ± 4 wt.% phyllosilicates and 51 ± 25 wt.% amorphous components (Bristow et al., 2018). If the mineralogy of Sutton Island is just a continuation of the Murray mineralogy in the surrounding stratigraphic members, we should expect to see a continuation of the weak ~ 860 nm absorption feature attributed to Fe^{3+} in hematite observed in Karasburg in the Sutton Island Mastcam data. Hematite has been hypothesized to have formed throughout the bedrock of the Murray formation through interactions with oxidizing fluids, either during deposition of the sediments in an oxidizing shallow lake environment (Hurowitz et al., 2017), during early diagenesis as a cement in a relatively porous sediment (Horgan et al., 2020), or during other early interactions with acidic and oxidizing fluids (Rampe et al., 2017).

2.3. Diagenetic Features

The effects of diagenesis have been observed throughout the Murray and Stimson formations, likely due to both early (before burial and lithification) and late (after lithification) diagenesis. Evidence for diagenesis includes late-stage silica-rich alteration halos (Frydenvang et al., 2017; Yen et al., 2017), polygonal fractures (Kronyak et al., 2019), late-stage concretions (Sun et al., 2019), sulfate-enriched vein and fracture fills (Nachon et al., 2014),

early diagenetic sulfate bedrock enrichment (Rapin et al., 2019), and bedrock color variations, or bleaching, due to dissolution and reprecipitation of hematite (Horgan et al., 2020).

Desiccation cracks have been well documented in the Old Soaker and nearby Squid Cove outcrops in SI and are indicative of subaerial exposure (Stein et al., 2018). Similar features have been observed elsewhere in SI, but these candidate mud cracks were not imaged at a small enough scale to determine if they have been filled with sediment, which is necessary to determine if they formed through desiccation or another process (Rapin et al., 2019). The ridges along polygonal fractures likely formed after the desiccation of the surface layer when sediment from an overlying bed was deposited along these mud cracks and later lithified. Ca-sulfates that sometime appear along these fractures or cross-cutting polygons likely formed after these desiccation cracks were lithified and buried when diagenetic fluids permeated through overlying sediments, possibly along fractures which may have propagated upwards from the desiccation cracks below (Stein et al., 2018).

Mineral-filled fractures are present throughout the Murray. Because the fractures themselves must have formed after lithification of the sediments, any mineral fill must be late diagenetic (e.g., Forni et al., 2015, 2016; Kronyak et al., 2019; Nachon et al., 2014, 2017; Rapin et al., 2016). Ca-sulfate veins are observed filling fractures in bedrock between bedding planes as well as cross-cutting beds, likely deposited by diagenetic fluids enriched in CaO and SO₃ (e.g., Forni et al., 2015, 2016; Nachon et al., 2014, 2017; Rapin et al., 2016). Silica rich alteration halos around some fractures have also been observed cross cutting the Stimson and Murray formations and are evidence of late diagenetic alteration by a different fluid than the fluid that formed the Ca-sulfate veins (Frydenvang et al., 2017; Yen et al., 2017).

MSL has encountered nodules and concretions throughout Mt. Sharp, likely both early and late diagenetic in origin (Grotzinger et al., 2014; Stack et al., 2014; Sun et al., 2019). Concretions of varying morphology appear throughout the Murray formation, including spherules, dendrites, flat, lamination-enhancing, and irregular morphologies. The Sutton Island and Blunts Point members are dominated by dark gray irregular and flat concretions of variable sizes and morphologies (Figure 2). Concretions with flat morphologies, which are more common in Sutton Island than elsewhere in the Murray (Sun et al., 2019), exhibit elevated Mn and P near the boundary of Sutton Island and Blunts Point (Meslin et al., 2018; Thompson et al., 2020). Significant variability in the size, texture, and chemistry can be seen in these features which suggests that they were precipitated during multiple distinct fluid events, possibly both early and late in timing (Sun et al., 2019).

2.4. Bedrock Chemistry

Data from the ChemCam and APXS instruments can be used to study changes in bedrock chemistry with elevation, or chemostratigraphy (Figures S2 and S3 in Supporting Information S1). Bedrock chemistry is calculated after removing any obvious diagenetic features such as veins, inclusions, and nodules from the dataset (Frydenvang et al., 2020; Mangold et al., 2019). The major element bulk chemistry of the Murray formation remains relatively constant (Table S1 in Supporting Information S1; Berger et al., 2020; Frydenvang et al., 2020; Mangold et al., 2019; Thompson et al., 2020); however, one stratigraphic region that does stand out in bedrock chemistry is the boundary between the Sutton Island and Blunts Point members (Figures S2 and S3 in Supporting Information S1). In this interval, bedrock is depleted in Si, K, and Cr and enriched in Fe, Mn, Mg, and Zn in addition to low FeO/MnO in APXS observations (Thompson et al., 2020). ChemCam data show similar depletions in SiO₂, K₂O, Na₂O Al₂O₃, TiO₂, Li and Rb and enrichment in Mn and MgO at this contact (Frydenvang et al., 2020). Elevated levels of Fe, Mn, and Mg are observed jointly within dark-toned layers in this region and certain dark-toned features also exhibit enhanced P in Fe-rich targets (Meslin et al., 2018; Thompson et al., 2020). Some hypotheses for the elevated Mn and Mg enrichment in this interval include precipitation of Mn-oxide in oxic lake waters (Gasda et al., 2019) or later diagenetic alteration (Meslin et al., 2018; Rapin et al., 2019).

Sutton Island also shows relatively elevated levels of Li and an increased Chemical Index of Alteration (CIA) (Table S1 and Figure S2 in Supporting Information S1; Frydenvang et al., 2020; Mangold et al., 2019). The CIA is determined from the molar ratio of Al₂O₃ over the summation of the compounds Al₂O₃, CaO, Na₂O and K₂O (Fedo et al., 1995; Nesbitt & Young, 1982), where higher values of this ratio can indicate leaching of mobile cations and thus a greater degree of chemical alteration over time. Increased CIA and Li content have been shown to be related to increases in clay mineral content in terrestrial rocks (Nesbitt & Young, 1982). Increased clay mineral content could be due to increased chemical weathering in a more open-system (Bristow et al., 2018). CIA

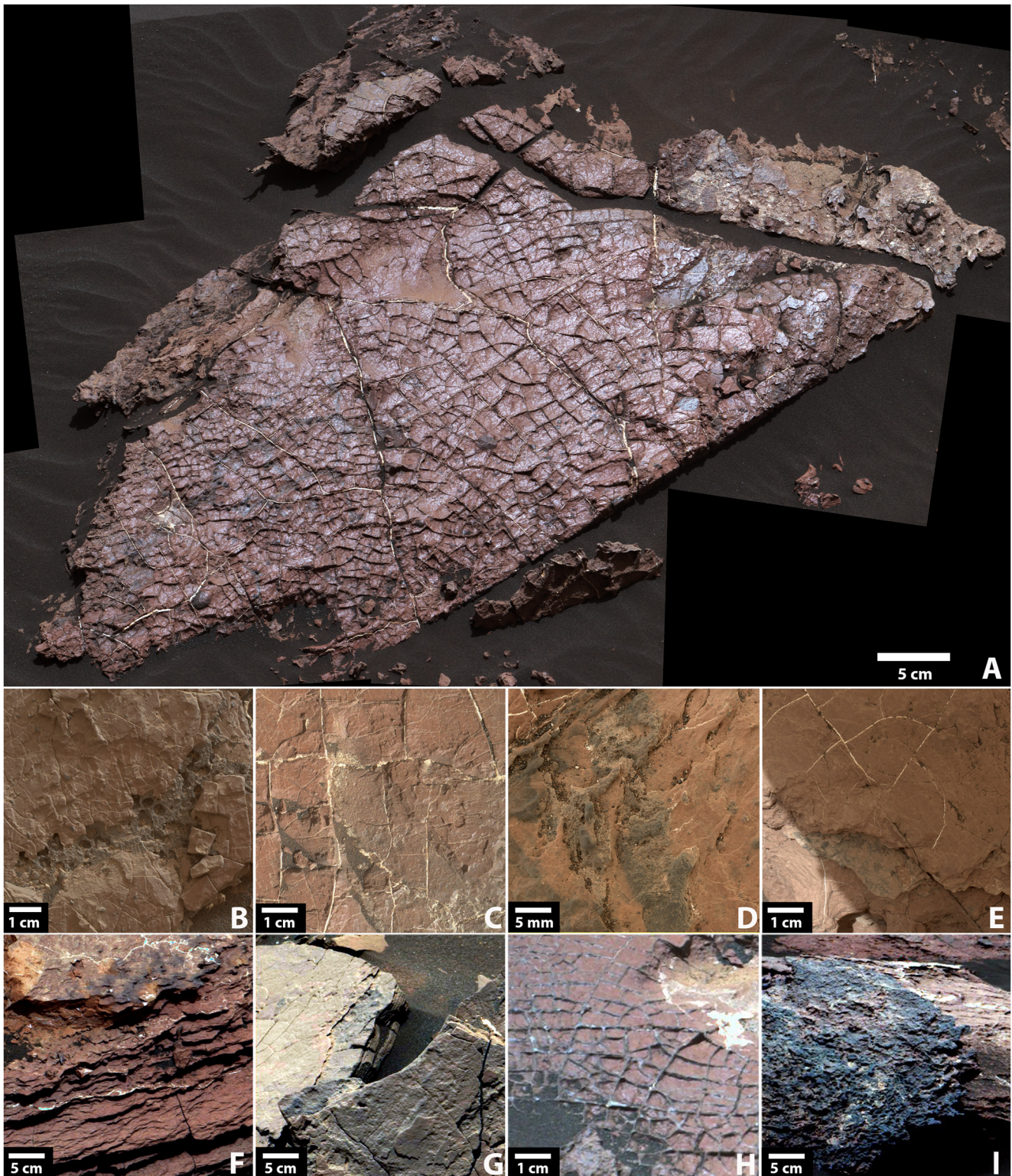


Figure 2. Diagenetic features in Sutton Island shown by the Mars Hand Lends Imager (B–E; MAHLI) and in Mastcam R0 enhanced color images (F–I) include (B and E) possible and (A, C, and H) confirmed desiccation cracks, (F) irregular mottling, (G–I) fracture fills, (G) flat concretions, and (I) outcrop coatings (A) Mastcam stereo mosaic (Sol 1,555 mcam07981) of Old Soaker (B) MAHLI Sol 1,668 Morancy Stream. (C) MAHLI Sol 1,566 Bar Island. (E) MAHLI Sol 1,589 Cape Elizabeth. (F) Sol 1,624 mcam08347. (G) Sol 1,693 mcam08822. (H) Sol 1,566 mcam07988. (I) Sol 1,596 mcam08130.

reflects weathering in an open system rather than isochemical alteration and does not take into account variation in Si (Mangold et al., 2019).

In addition to late-diagenetic light toned veins that are pervasive throughout the bedrock of the Murray Formation, there are also certain horizons where the bedrock itself is enriched in both Ca- and Mg-sulfates. Bedrock is enriched with Ca-sulfate between $-4,370$ and $-4,200$ m from the Sutton Island member and into the Blunts Point member, which contrasts with only sporadic enrichment detected elsewhere in the Murray formation (Rapin et al., 2019). Additionally, an enrichment in Mg-sulfate was detected in bedrock in a very thin stratigraphic interval of less than 10 m around an elevation of $-4,287$ m near the boundary between Sutton Island and Blunts Point. Mg-sulfate enrichment is more commonly found in dark and red-toned bedrock horizons while Ca-sulfate enrichment is more common in light-toned bedrock horizons. The enrichment of Sutton Island with evaporitic materials along with sedimentological features such as desiccation cracks suggests that this region may have been deposited in an evaporitic or lakeshore setting with increased subaerial exposure (Rapin et al., 2019).

2.5. Sutton Island: A Unique Stratigraphic Interval

These chemical and sedimentological observations suggest that the Sutton Island member may be compositionally distinct due to a different depositional and/or diagenetic history compared to neighboring parts of the Murray formation. This area likely experienced increased desiccation and weathering, and the facies are indicative of a change in depositional environment from the surrounding Murray. Because of the paucity of drilled samples in this area, we are unable to quantitatively study mineralogy of this unique region beyond the single sample collected at the base of Sutton Island. Without this information, it is difficult to constrain the timing and chemistry of lake waters and diagenetic fluids that formed the enriched bedrock and diagenetic features we see today.

In this study, we use Mastcam multispectral data from individual bedrock targets and trends in spectral parameters compared with chemostratigraphy from ChemCam and APXS to better constrain the Fe-bearing mineralogy of the Sutton Island member. In this unique region, we expect to see a change in mineralogy from surrounding parts of the Murray related to the distinct depositional environment and/or alteration history suggested by other data sets.

3. Methods

3.1. Mastcam Multispectral Analysis

Mastcam is a multispectral imager composed of two cameras (100/34 mm focal lengths) on the mast of the Curiosity rover, with RGB Bayer filters mounted on the Kodak KAI-2020CM CCD detector (Malin et al., 2017). Mastcam acquires multispectral images using additional filters mounted in a filter wheel that are rotated sequentially in front of the detectors. With 12 spectral channels (3 broadband Bayer filters and 9 unique narrowband filters) between 445 and 1,013 nm, Mastcam multispectral images can be used to constrain Fe-bearing minerals and their oxidation states.

Images are calibrated to relative reflectance using spectra from a target onboard the rover. Images are converted from radiance to radiance factor (I/F) by division by a solar and atmospheric transmission spectrum derived from imaging of the calibration target onboard the rover immediately after or before imaging the science target (Bell et al., 2017; Wellington et al., 2017).

In order to assess spectral diversity within a scene, decorrelation stretches (DCS) of the R3 (805 nm), R1 (527 nm) and R2 (447 nm) narrowband channels were applied to multispectral images from the M100 camera. A DCS can help reveal diversity and identify spectrally homogenous ROIs within a multispectral image of an outcrop by suppressing differences in albedo and enhancing color separation (e.g., Farrand et al., 2007, 2016; Gillespie et al., 1986; Horgan et al., 2020). Average I/F spectra of homogenous and relatively dust free areas were extracted from regions of interests (ROIs) in both M34 (left eye) and M100 (right eye) images. To create a joined spectrum from the M34 and M100 spectra, each M100 spectrum was scaled to the M34 spectrum at 1,013 nm. The spectra from both eyes were then averaged at overlapping wavelengths. Convention for selecting ROIs and generating spectra is similar to previous studies (Fraeman, Edgar, et al., 2020; Fraeman, Johnson, et al., 2020; Horgan et al., 2020; Jacob et al., 2020; Rice et al., 2022; Starr et al., 2019; Wellington et al., 2017). Variation bars represent the standard deviation within an ROI and is larger than the instrumental error (Bell et al., 2017).

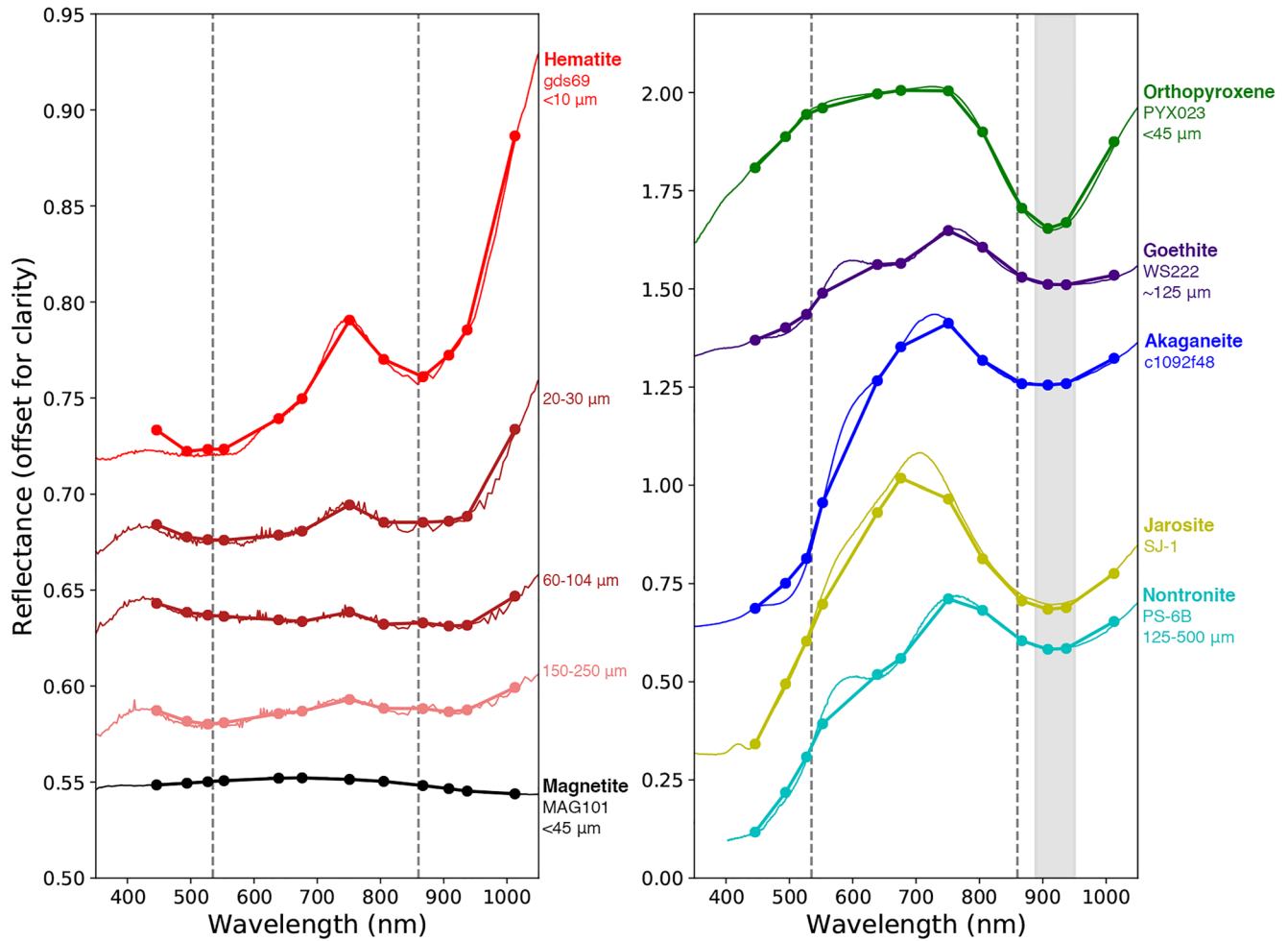


Figure 3. Laboratory spectra of iron oxides with varying grain size (left) and common Fe-bearing minerals with ~ 900 nm absorption bands (right) convolved with Mastcam multispectral bandpasses (Bell et al., 2017) and offset for clarity. Vertical dashed lines indicate locations of absorptions at 860 and 535 nm that are commonly associated with Fe^{3+} in hematite and the Gy bar indicates a range of absorption features centered at or beyond 900 nm. Spectra were sourced from the USGS Spectral Library (Clark et al., 2007), RELAB (Pieters, 1983), and the University of Winnipeg's Centre for Terrestrial and Planetary Exploration's spectral database.

We also incorporate two Mastcam spectral datasets collected within and beyond the Sutton Island member for efforts outside of this study, and these spectra are called out separately on all plots where they appear. These data include spectra previous published by Horgan et al. (2020) and Rice et al. (2022). These datasets are shown in the band parameter trend plots to both ensure that our Sutton Island database is representative of the true variability in the bedrock, and for comparison of Sutton Island bedrock spectral properties to those of nearby stratigraphic members.

3.2. Comparison With Lab Minerals

In order constrain the mineralogy of targets observed in Mastcam multispectral data, we use previously published data on lab minerals with diagnostic spectral features in the range of Mastcam (Figure 3). Iron oxides exhibit electron transition features at 405–410 nm (${}^6A_1 \rightarrow {}^4A_1$, 4E_1), 488–493 nm (electron pair transition), 650–710 nm (${}^6A_1 \rightarrow {}^4T_2$), and 848–906 nm (${}^6A_1 \rightarrow {}^4T_1$; Morris et al., 1985). Most iron oxides display these absorption features at relatively similar wavelengths that makes them hard to distinguish from each other. However, the ${}^6A_1 \rightarrow {}^4T_1$ transition in hematite is centered at somewhat shorter wavelengths, ~ 860 – 880 nm, which is unique to this mineral (Scheinost et al., 1998). Most other iron oxides exhibit similar broad absorption features centered at ≥ 900 nm (Figure 3 and Figure S4 in Supporting Information S1). Additionally, while most Fe-oxides share an absorption

feature near 480–550 nm, hematite exhibits a steeper inflection at ~535 nm relative to other Fe-oxides due to its ${}^6A_1 \rightarrow {}^4A_1$, 4E_1 and pair ($2({}^6A_1) \rightarrow 2({}^4T_1)$) transitions (Sherman & Waite, 1985).

Fe-smectites, such as nontronite, display broad absorption features centered near 920 nm due to Fe^{2+} and Fe^{3+} electron transitions and an additional absorption feature near 670 nm (e.g., Jacob et al., 2020), which distinguishes them from most Fe-oxides but is difficult to discern with the spectral resolution and spectral sampling of the Mastcam filters (Figure 3). Several Fe-sulfates exhibit a band >900 nm, typically along with a sharp band near 430 nm and a band near 500–600 nm (e.g., Cloutis et al., 2006). Broad absorptions due to crystal field transitions of Fe^{2+} in silicate minerals occur near 900–1,200 nm in mafic silicates like olivine, pyroxene, and glass (e.g., Cloutis et al., 2006).

We used Mastcam multispectral data to constrain bedrock Fe-mineralogy both by visual comparison to the lab spectra shown in Figure 3 and also by studying trends in quantitative band parameters. These parameters include band depth at 527 nm (BD527) and 867 nm (BD867; Fraeman, Edgar, et al., 2020; Fraeman, Johnson, et al., 2020; Wellington et al., 2017) and band minimum location in the range of 751–1,012.5 nm (corresponding to Mastcam channel wavelengths). Additionally, we calculated the band center location of the absorption in the 751–1,012.5 nm range by (a) dividing each spectrum by a linear continuum fit to 751 and 1,012.5 nm, (b) fitting a second order polynomial to the continuum removed reflectance in each filter and then (c) finding the wavelength location of the minimum of that polynomial. We recognize these modeled band centers are subject to uncertainties on the order of the ~10 nm bandpass of the narrow band filters used by Mastcam. We have also applied this technique to hyperspectral lab data as well as lab data convolved with the Mastcam filters (Figure 3), and we found that this method applied to lab mineral spectra convolved with Mastcam filters more accurately matched the band center of the hyperspectral data than simply determining the band minimum in the Mastcam channels (Figures S4 and S5 in Supporting Information S1). Band depths at both the band minimum and modeled band center are calculated by determining the percent difference between the reflectance at the minimum Mastcam channel wavelengths or of the fitted polynomial and a straight line between two shoulders.

3.3. Chemistry Data

ChemCam provides remote observations of chemical composition of targets using laser-induced breakdown spectroscopy (LIBS; Wiens et al., 2012). A laser on the instrument fires at a target and generates a plasma at the target so that elemental emission lines can be measured. ChemCam LIBS spot sizes are typically 0.35–0.55 mm in diameter, and ChemCam is sensitive to major elements (Fe, Na, Mg, Al, Si, K, and Ca), minor and trace elements at varying limits of detection (Li, Ti, Cr, Mn, Ni, Cu, Zn, Rb, As, Sr, Cd, Cs, Ba, and Pb; Maurice et al., 2012), and volatiles and halogens (O, S, C, P, H, Cl, F) if present in sufficient proportions, typically from 1% to 10% in elemental weight depending on elements (e.g., Forni et al., 2015). Quantification of major elements can be done by multivariate analyses using a series of emission lines per element, and comparing them to >400 standards analyzed in a testbed in similar conditions as on Mars (Clegg et al., 2017). The ChemCam instrument can also collect passive spectra calibrated to relative reflectance from targets without utilizing LIBS. These passive mode (Johnson et al., 2015, 2016) spectra range from 400–840 nm with a spatial resolution of 0.65 mrad corresponding to fields of view of 1.3 mm at a distance of 2 m. The ChemCam instrument also possesses a Remote Micro-Imager (RMI) which provides context for LIBS targets. In this study, RMI images were used to locate ChemCam targets within Mastcam images.

The Alpha Particle X-ray Spectrometer (APXS) utilizes X-ray fluorescence (XRF) and particle-induced X-ray emission (PIXE) to determine elemental composition (Campbell et al., 2012). APXS acquires data from spots typically 1.5–2 cm in diameter, and is sensitive to a larger number of major, minor, and trace elements than ChemCam. We made use of the APXS oxide abundance data, provided as a percentage of total composition, that are archived in the Planetary Data System (PDS). The APXS footprint (~2.5 cm) is much larger than the ChemCam footprint (typically ~350–550 μ m in diameter at distances of 2–5 m) which allows for analysis of smaller scale features in bedrock targets such as individual grains and small diagenetic features. An average of individual ChemCam points on given targets is done to provide an equivalent bulk chemistry and avoid local heterogeneities (Mangold et al., 2019). Additionally, the vertical depth that contributes to the signal is different as ChemCam LIBS ablates targets while APXS is limited to the very near surface and utilizes the Dust Removal Tool (DRT) to decrease the amount of dust on bedrock targets. Because ChemCam and APXS can observe the abundance of

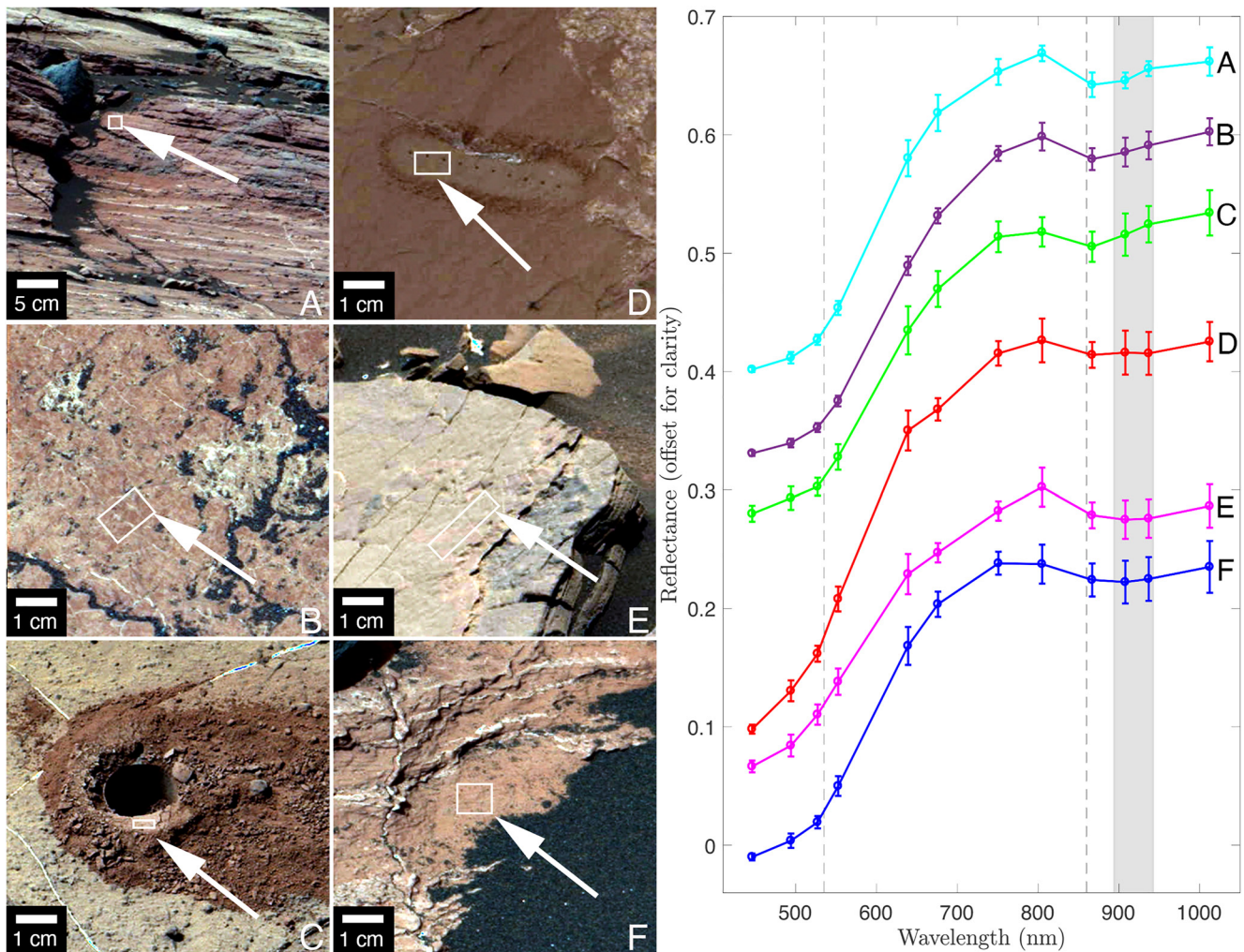


Figure 4. Some spectra in the Sutton Island member (A: Sol 1,608 mcam08215; B: Sol 1,608 mcam08214) exhibit strong absorption features at ~ 860 and ~ 535 nm (dashed lines), indicative of fine-grained crystalline red hematite, including the drill tailings for the Sebina sample (C: Sol 1,496 mcam07566). However, much of the bedrock in upper Sutton Island (D: Sol 1,725 mcam09004; E: Sol 1,693 mcam08822; F: Sol 1,610 mcam08231) exhibits absorption features centered at or beyond 900 nm (gray bar) that are inconsistent with hematite. Mastcam R0 images are shown on the left, with regions of interests (ROIs) used to extract local average spectra outlined in white.

different elements and compounds in the bedrock, they make an excellent complementary data set to study trends in bedrock chemistry along the rover traverse.

4. Results

4.1. Spectral Properties and Diversity

Spectra collected from bedrock in the Sutton Island member generally fall into two distinct classes (Figure 4) with another class found only in dark likely diagenetic features (Figure 5). The first class of spectra (Figures 4a–4c) show moderate to deep bands centered at 867 nm and steep slopes at short wavelengths including a deep absorption at 527 nm, consistent with fine-grained crystalline red hematite (Morris et al., 1985). Similar spectra are common throughout the Murray on red bedrock targets partially cleared of dust by the DRT (Rice et al., 2022; Wellington et al., 2017). Spectra from Sebina bedrock and drill tailings fall into this class, which is consistent with hematite detections at this site by CheMin (Bristow et al., 2018; Rampe et al., 2020). Mastcam-convolved spectra of a limited sample set of two akaganeite spectra show similar band centers near 870 nm (Figure S4 in Supporting Information S1). Akaganeite is present in some locations in the Murray (1.2–6 wt.%), but not in the

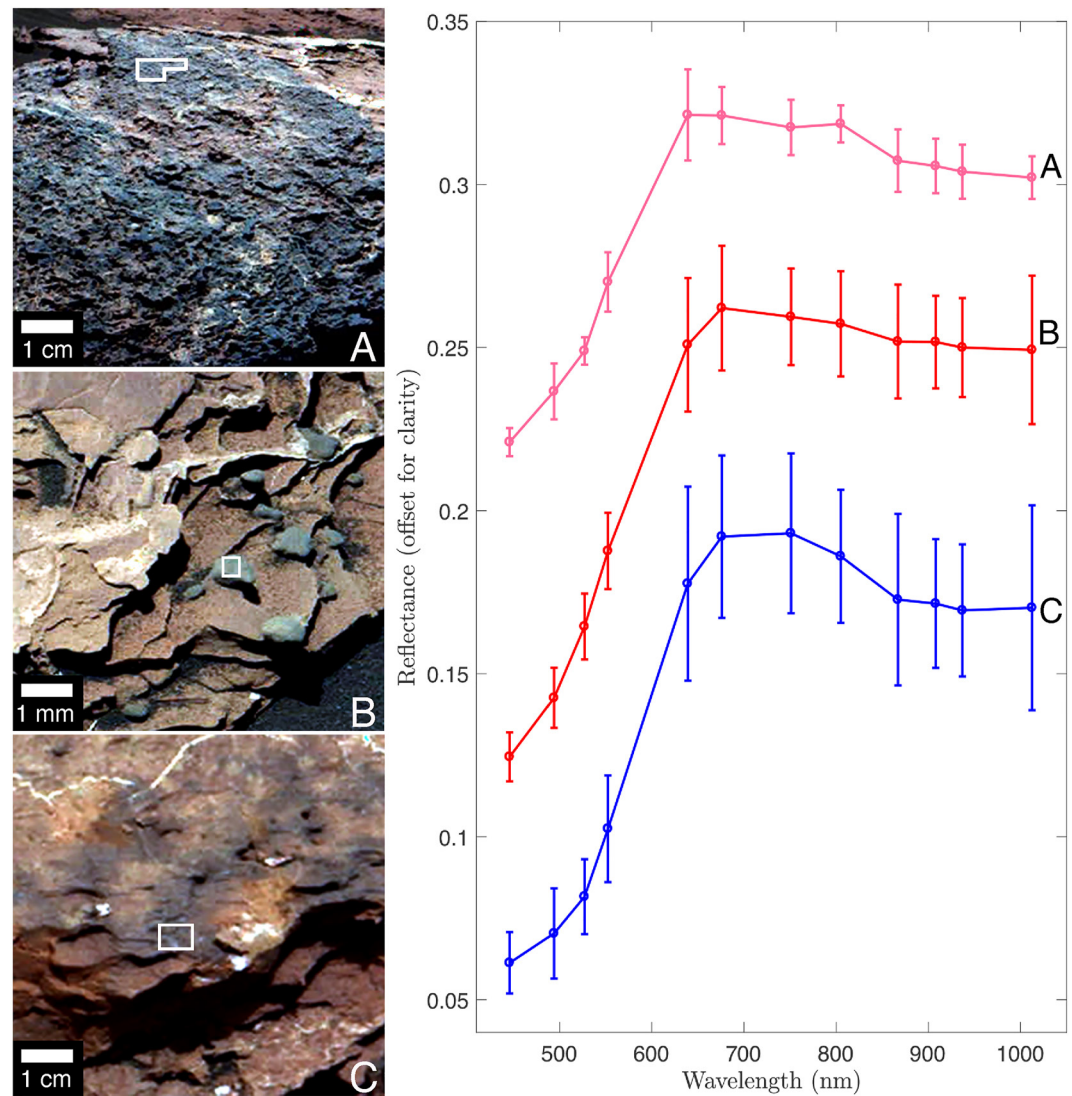


Figure 5. Dark gray features in Sutton Island bedrock display a variety of morphologies (Figure 2) and many exhibit similar spectral features with reflectance peaking around 650–700 nm and no obvious band minimum between 800 and 1,000 nm. RO images taken by Mastcam of these targets are shown on the left, with regions of interests (ROIs) used to extract local average spectra outlined in white. (A: Sol 1,596 mcam08130; B: Sol 1,745 mcam09118; C: Sol 1,624 mcam08347).

samples in or around Sutton Island, including Sebina, and so hematite is more likely to be responsible for 860 nm bands in and around Sutton Island.

The second spectral class (Figures 4d–4f) exhibits a steep slope at short wavelengths, a reflectance peak centered at either 751 nm or 805 nm, and a band minimum at 908 nm or greater. Additionally, the 527 nm absorption is weaker in this class (Figure S6 in Supporting Information S1). In lab spectra of minerals convolved to Mastcam wavelengths, band minima at 910 and 935 nm are not consistent with hematite and instead occur in other Fe-bearing minerals, including Fe/Mg-smectite (910 or 930 nm), jarosite (910 nm), and goethite (910 nm), or a mixture of these phases (Horgan et al., 2020, Figure 3 and Figure S4 in Supporting Information S1). Of these minerals, Fe/Mg-smectite has been detected both from orbit (Carter et al., 2016; Fraeman et al., 2016) and in situ (Bristow et al., 2018; Jacob et al., 2020) at elevated abundances (19 ± 4 wt.%) in Sebina, the single CheMin analysis at the base of the Sutton Island member. Jarosite has been detected at very low abundances (1–2.3 wt.%) in some CheMin analyses (Rampe et al., 2020) and ChemCam passive spectra (Johnson et al., 2016) elsewhere in the Murray formation but has not been observed in SI, nor is there a stoichiometric increase in K and S in the APXS data, which might be expected if jarosite were present. Goethite has not been identified from orbit or in

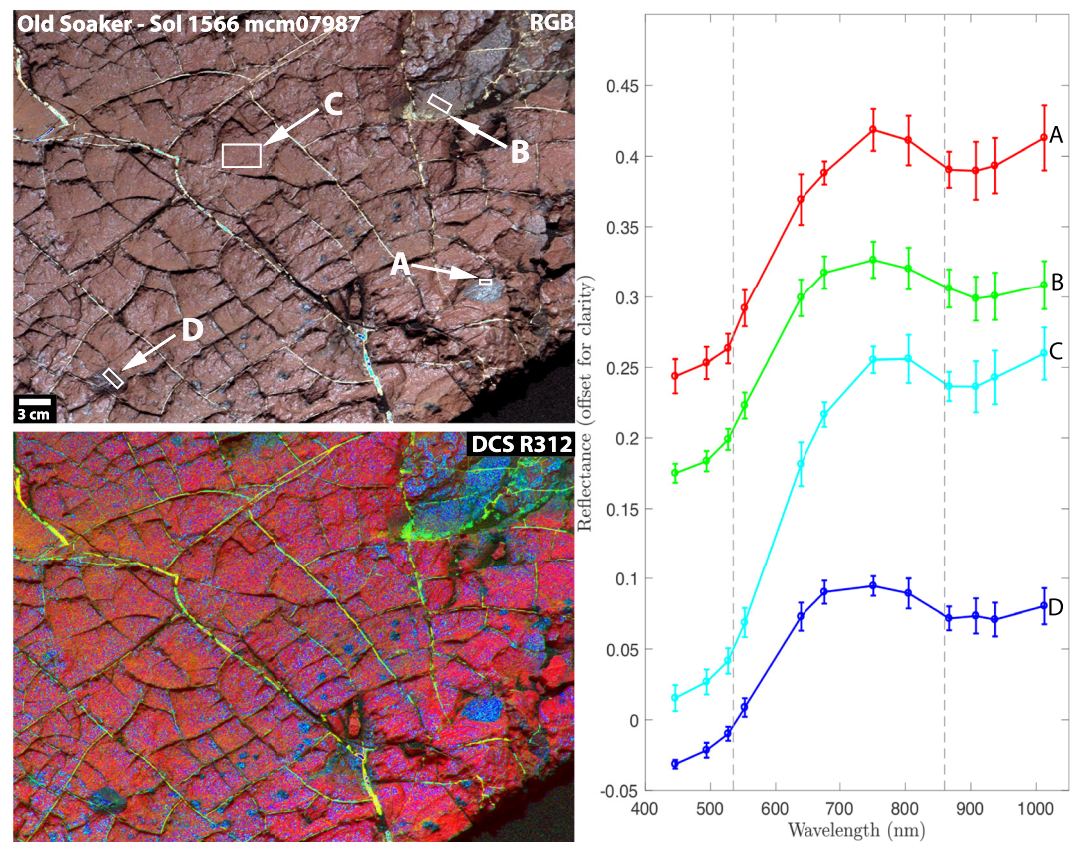


Figure 6. Old Soaker imaged by Mastcam on Sol 1,566 in the Sutton Island member, shown in enhanced R0 color and decorrelation stretches (DCS) of filters R312. Spectra of regions of interests from a reflective round inclusion (A), an irregular dark inclusion (B), red bedrock (C), and a rounded dark inclusion (D). Old Soaker exhibits some of the most diverse alteration features including desiccation cracks with variable sulfate or dark mineral fill and a variety of dark inclusions.

situ in the Murray formation, but has been detected in the stratigraphically higher Carolyn Shoemaker formation (Rampe et al., 2022). Thus, we hypothesize that this spectral signature is primarily due to Fe/Mg-smectite, although contributions from the substantial amorphous component (51 ± 25 wt.% in Sebina) and variations in grain size likely influence the spectra to an uncertain degree.

The third class of spectra (Figure 5) exhibits a peak reflectance near 670 nm and flattening or a long blue slope toward longer wavelengths, with no apparent absorption bands centered between 800 and 950 nm. Reflectance usually peaks in the 676 nm or 751 nm channels. In Sutton Island, these spectra were only detected in dark gray features (Figure 2) that occur as apparent coatings on bedrock outcrops, between bedrock layers, or as small inclusions within bedrock.

Many outcrops within the Sutton Island member show significant variation in color and morphology, which is enhanced with a DCS. The type example is the rock Old Soaker (Figure 6), which exhibits Ca-sulfate veins and desiccation fracture fill (green in DCS), red bedrock (magenta in the DCS) and dark-toned desiccation fracture fill and concretions (blue in the DCS). While the bedrock color appears relatively homogenous in the approximate true color, the DCS reveals some mottling and many more diagenetic inclusions. Spectra of red bedrock at Old Soaker exhibit >900 nm bands similar to the second class (Figure 6c), as does a very reflective and rounded blue-gray inclusion (Figure 6a). Other dark-toned features exhibit spectra consistent with variations on the third spectral class (Figures 6b and 6D), suggesting that not all diagenetic inclusions and mottling share the same composition. The significant spectral variability visible in the DCS here is not unique to Old Soaker, as many outcrops in this region display similarly diverse spectra, which is what makes them appear mottled when a DCS is applied.

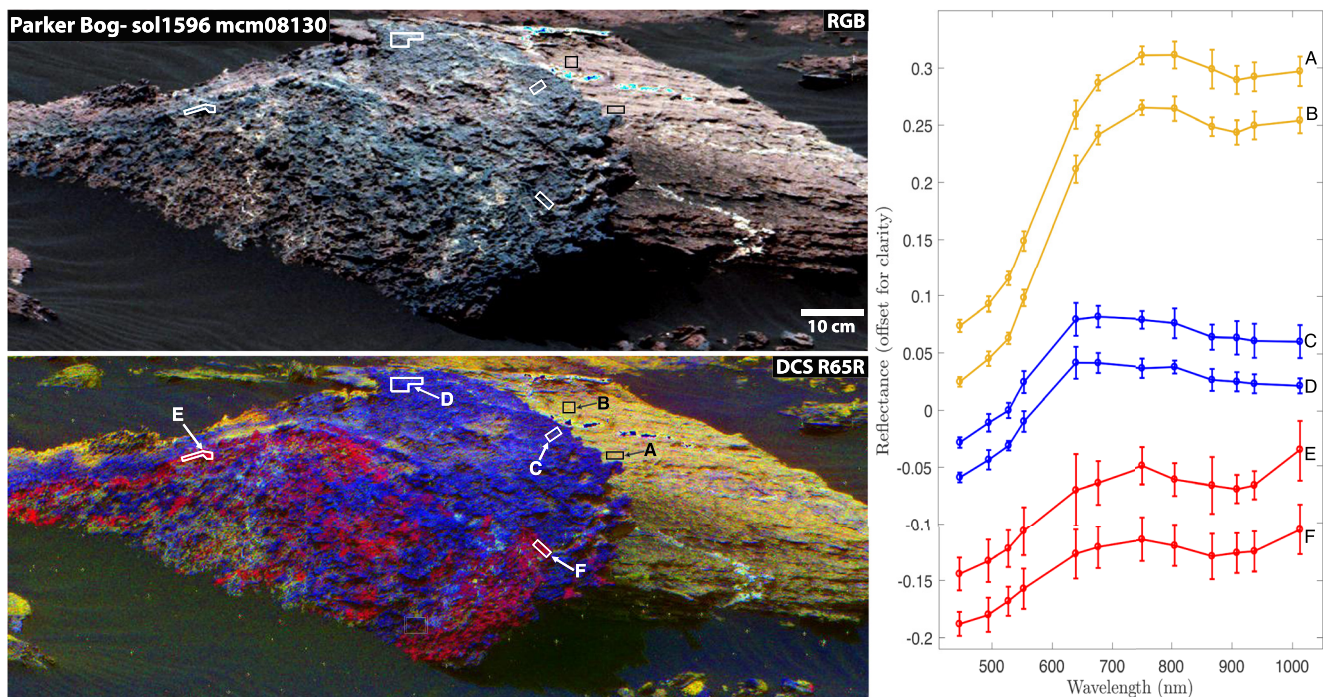


Figure 7. Parker Bog imaged by Mastcam on Sol 1,596 in the Sutton Island member, shown in enhanced R0 color and decorrelation stretches (DCS) of filters R65R, where R in the DCS is the red Bayer filter in the right eye. Spectra of regions of interests (ROIs) shown on right and color of spectra correspond to color in the DCS. Dark toned regions which appear relatively homogenous in the RGB R0 Bayer filters image show more diversity in the DCS.

Some Mastcam images collected in Sutton Island that appear homogenous in RGB Bayer filter color images show variability at longer wavelengths. The target Parker Bog imaged on Sol 1,596 has a dark gray coating that appears to cover most of the outcrop (Figure 7). While the gray areas appear relatively homogenous in approximate true color or even enhanced color Bayer filter (R0/L0) images, a decorrelation stretch including longer wavelength images (e.g., R6 and R5) shows that this surface is actually highly mottled. Spectra collected from the red regions of the DCS exhibit deep and very broad absorptions near 867 nm and reflectance peaks at 751 nm (Figures 7e and 7f), indicative of fine-grained crystalline hematite (Morris et al., 1985). Spectra taken from blue parts of the DCS appear similar to the third class of spectra (Figure 5) with peak reflectance near 670 nm, a blue slope to long wavelengths, and no apparent absorption band centered between 800 and 950 nm (Figures 7c and 7d), consistent with a more ferrous mineral (e.g., olivine, pyroxene, magnetite, mixed valence phyllosilicates) or coarse-grained Fe-oxides (e.g., hematite; Horgan et al., 2020, Figure 3). Adjacent bedrock in Parker Bog is typical of Sutton Island, with a pink to red color, reddish visible wavelength slope, a broad absorption band centered near ~900 nm, and a reflectance peak at 805 nm (Figures 7a and 7b).

Gradations in bedrock color/tone are also apparent in some outcrops, typically with color transitioning from red to tan. Differences in the color and tone of bleached outcrops are enhanced in a DCS image of target Jemmland (Figure 8). Color changing from red to tan correlates with progressively weaker red slopes <750 nm, but only minor differences in the depths and shapes of absorption features (Figure 8). This outcrop also contains gray features that are more apparent in the DCS that exhibit spectral properties resembling other dark diagenetic features visible elsewhere (Figure 5) with some additional absorption (Figure 8d). Similar color differences from red to gray or tan have been observed on the Vera Rubin ridge, where they were interpreted as due to remobilization and coarsening of hematite grains by diagenetic fluids and referred to as bleaching (Horgan et al., 2020). However, on VRR bleached zones exhibited weak to no 860–900 nm bands. The retention of the strong ~900 nm bands across these color changes in SI suggests that there is an Fe-bearing phase responsible for the ~900 nm bands that is not affected by whatever process caused this color change.

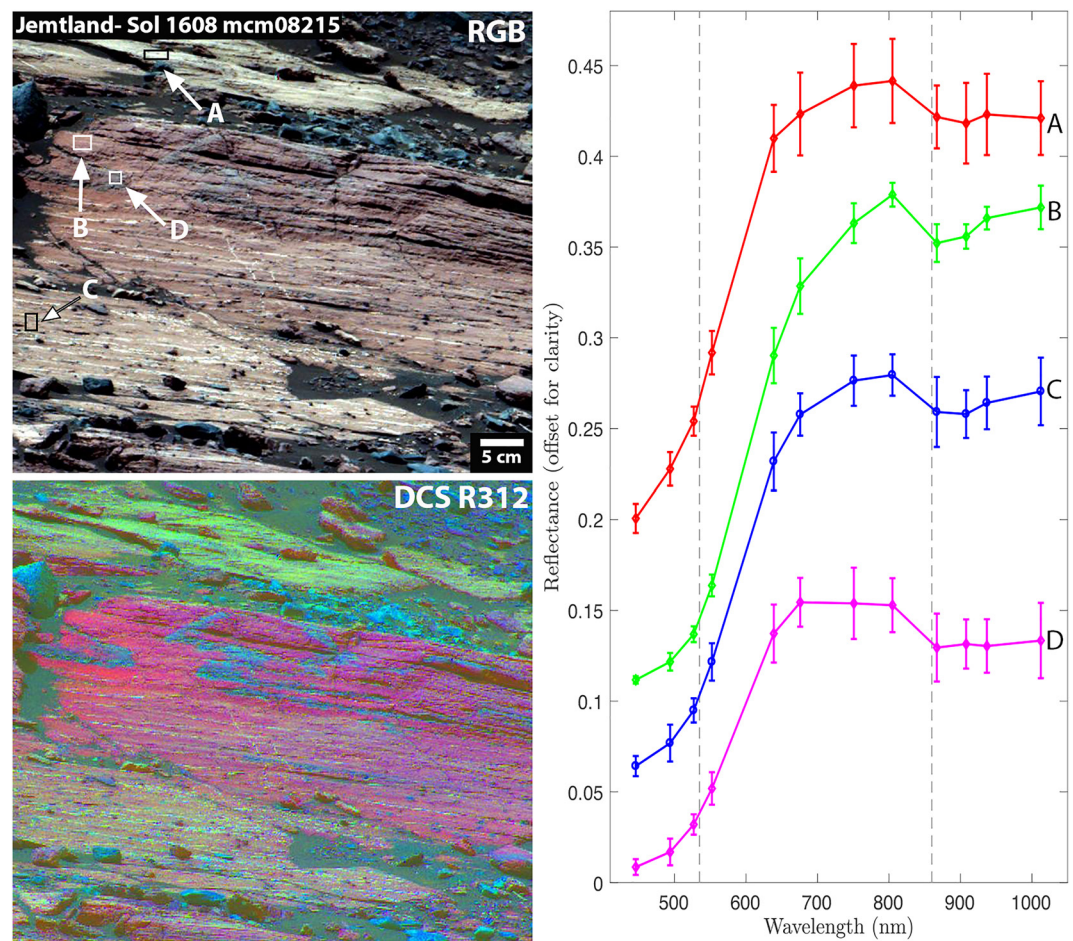


Figure 8. In target Jemmland imaged by Mastcam on Sol 1,608 near Ireson Hill shown in enhanced R0 color and decorrelation stretches (DCS) of filters R312, light and dark toned areas exhibit different spectral features. There are very subtle differences between the spectra collected from lighter toned bedrock (A and C) and the dark red toned bedrock (B), primarily that the red slope <750 nm is much steeper in the red bedrock. Dark gray parts of the bedrock exhibit peaks at ~700 nm and stand out in the DCS (D).

4.2. Spectral Trends With Elevation

Figure 9 shows trends in band minimum, fitted band center, and band depth versus target elevation for Mastcam spectra collected from bedrock in the Sutton Island member and neighboring parts of the Murray formation in this study as well as published spectra from Horgan et al. (2020) and Rice et al. (2022). Most Murray bedrock stratigraphically below Sutton Island and in VRR exhibit band minima at 867 nm, indicative of crystalline hematite (Horgan et al., 2020; Wellington et al., 2017). In contrast, band minima at 908 and 937 nm are much more common in the Sutton Island and Blunts Point. Band center position reflects this shift but shows more subtle trends. Band center position appears to increase with elevation in the Sutton Island member, reaching a local maximum between Old Soaker and the boundary with Blunts Point (−4,280 m), from where it decreases gradually toward VRR (Figure 9). Multispectral data collected in Sutton Island and Blunts Point from both dusty and dust cleared bedrock show this trend, indicating that the varying band center position is not due to dust cover (Rice et al., 2022; Starr et al., 2019).

The BD867 parameter mirrors the change in band center, as it increases from the boundary between Karasburg and Sutton Island and peaks near the outcrop Old Soaker (−4,335 m) and then decreases toward the boundary between Sutton Island and Blunts Point. The BD527 parameter follows a similar pattern, but it peaks slightly further upsection near the Parker Bog outcrop (−4,300 m; Figure 9). Additionally, spectra with lower BD527 values tend to have longer wavelength absorption features centered near 908 nm or greater (Figure S7 in

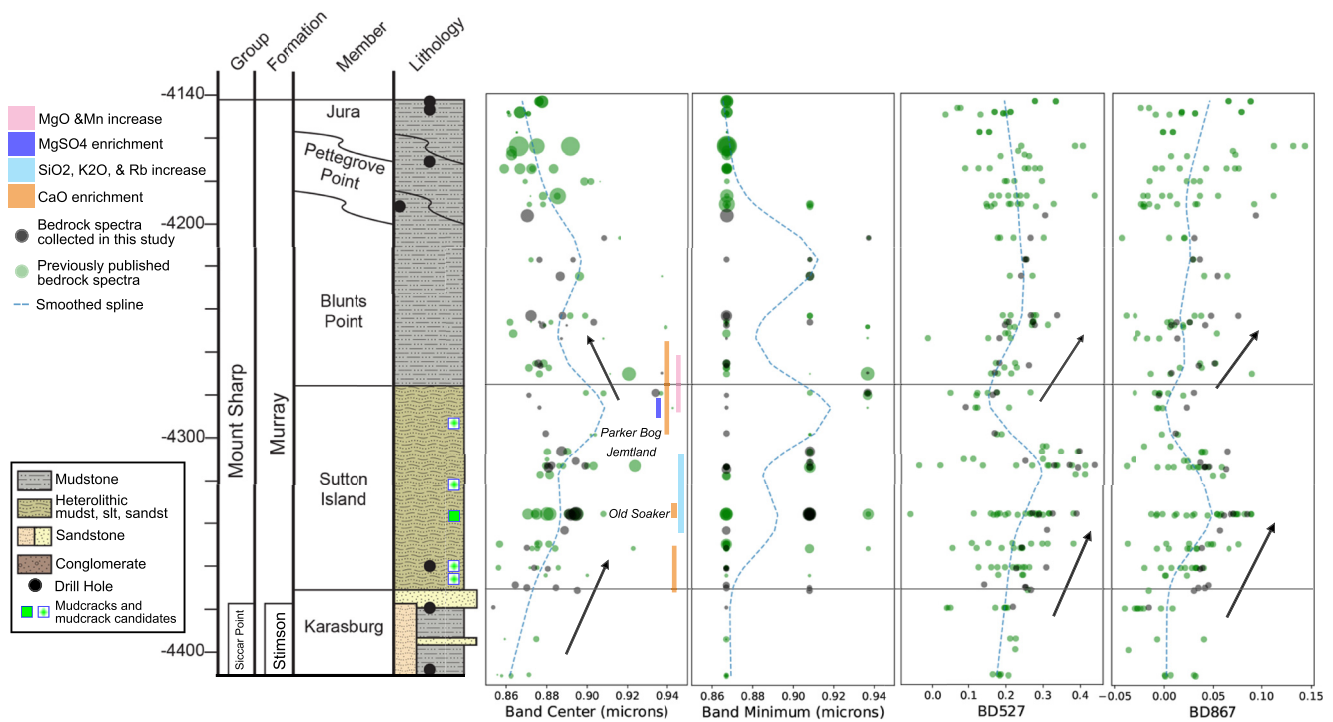


Figure 9. Trends in Mastcam spectral parameters versus elevation. Black points represent band parameters calculated from bedrock spectra collected in this study while green points are parameters calculated on previously published bedrock spectra (Horgan et al., 2020; Rice et al., 2022). Point sizes in modeled band center and minimum plots are scaled with band depth at the minimum or center, respectively (larger indicates deeper bands). Modeled band center shows trends in the position of the 860–900 nm iron oxide absorption feature with elevation more clearly than the minimum Mastcam filter in this range. Band center of this feature trends toward longer wavelengths with elevation in the Sutton Island member before decreasing upsection toward Blunts Point. Similar trends can be seen in the location of the band minimum and the values of BD527 and BD867. A smoothed spline helps to show trends in the data with elevation. Stratigraphic column is included for context on the left (modified from Fedo et al., 2019), along with important chemostratigraphic intervals and the location of desiccation cracks.

Supporting Information S1), suggesting that the phase that is causing the >900 nm band is likely not one with a strong band near 527 nm (e.g., hematite, goethite, akaganeite; Figure 3, Morris et al., 1985). This is consistent with either Fe/Mg-smectite or jarosite as the causes of the >900 nm band and supports our hypothesis that this band in Sutton Island is due to Fe/Mg-smectites.

Comparison to ChemCam passive hyperspectral data from the same rock targets show similar trends. The center and depth of the absorption feature in the range of 840–1,000 nm cannot be directly observed in ChemCam data, but the depth of this absorption can be inferred from the slope between 750 and 840 nm, where a more negative slope corresponds to a deeper absorption feature (Johnson et al., 2015). The absorption featured centered at 535 nm can be observed in ChemCam spectra (Johnson et al., 2015). Both of these parameters show similar trends with elevation as their Mastcam counterparts, increasing in depth and slope throughout Sutton Island until reaching a maximum at –4,300 m, near the Parker Bog outcrop, and dropping toward Blunts Point before increasing again toward VRR (Figure S8 in Supporting Information S1; Fraeman, Edgar, et al., 2020; Fraeman, Johnson, et al., 2020).

4.3. Comparisons to Chemical Datasets

Mastcam spectra can be used to detect a variety of Fe-bearing minerals, but other than a few exceptions such as hematite, it is difficult to distinguish between these minerals solely based on the location of absorption features (Scheinost et al., 1998). Incorporating data and trends in rock chemistry from the ChemCam and APXS instruments may help constrain the possible minerals. For example, if jarosite is present at significant abundances, we may expect an increase in sulfur, iron, potassium, or perhaps chlorine associated with the presence of akaganeite, which forms in chloride rich environments and incorporates chlorine into its structure.

Data from both the ChemCam and APXS instruments show increasing bulk rock abundances of MgO, from approximately 5–20 wt.% observed by ChemCam upwards through Sutton Island peaking at the boundary with Blunts Point (Frydenvang et al., 2020; Mangold et al., 2019; Thompson et al., 2020). Mn in ChemCam data and MnO in APXS data show similar trends as MgO, reaching a much greater maximum (CCAM: 1.6e–3 line area; APXS: 3.99 wt.%) at the boundary between Sutton Island and Blunts Point than elsewhere in the Murray. Both APXS and ChemCam show K₂O at a minimum (CCAM: ~0.5 wt.%; APXS: 0.3 wt.%) at the boundary between Karasburg and Sutton Island, peaking (CCAM: ~2.4 wt.%; APXS 2.3 wt.%) near the Old Soaker outcrop (–4,335), and then decreasing again reaching another minimum (CCAM: ~0.4 wt.%; APXS ~0.3 wt.%) near the boundary with Blunts Point (Figures S2 and S3 in Supporting Information S1). Additionally, increasing CIA through Sutton Island was observed, peaking near the Old Soaker outcrop and again at the boundary with Blunts Point where it slowly decreases toward VRR. The boundary between the Sutton Island and Blunts Point members corresponds to many of the variable diagenetic facies and spectral diversity described above. Of these various chemical trends, the two that mimic most closely the shift in band center in Mastcam spectra toward longer wavelengths are K₂O and CIA, both of which peak around Old Soaker, similar to the Mastcam parameter plots.

For completeness, we also directly compared APXS and ChemCam chemistry data with Mastcam multispectral data from the same points, where some weak to moderate correlations were observed (Figures S8–S11 in Supporting Information S1). However, this method is challenging because of the minimal overlap in targets between the datasets and differences in the nature and scale of these techniques (Text S1 in Supporting Information S1; Anderson & Bell, 2013). Thus, we observed weak to moderate correlations that generally support our conclusions based on the trend plots above, but are not diagnostic on their own (Figures S8–S11 in Supporting Information S1).

4.4. Summary of Mineral Interpretations

Mastcam multispectral data reveal disparities between the Sutton Island member and typical Murray formation. While bedrock spectra with absorption bands centered at 867 nm are standard in Mastcam spectra throughout the Murray (Horgan et al., 2020; Rice et al., 2022; Wellington et al., 2017), they are less common in the bedrock of Sutton Island and sporadic in Blunts Point. Fine-grained red crystalline hematite must be effectively absent (~<3 wt.%; Figure S5 in Supporting Information S1) in some parts of Sutton Island, otherwise it would dominate all relatively dust-free spectra and overpower absorption features of ferrous silicates due to hematite's strong pigmentary nature (Cornell & Schwertmann, 2003; Morris et al., 1985). Additionally, most of the bedrock spectra with longer wavelength band centers do not exhibit deep absorptions at the 527 nm channel associated with fine-grained crystalline hematite, goethite, and akaganeite (Figure S6 in Supporting Information S1; Scheinost et al., 1998). An alternative Fe-bearing mineral must be causing the observed absorption feature centered at >900 nm.

Several possible minerals have band centers located in the 890–950 nm range observed in Sutton Island. Band centers of these minerals were determined using the same methods used on Mastcam spectra but with lab spectra convolved with Mastcam spectral bandpasses (Figure 3 and Figure S4 in Supporting Information S1). These minerals include the ferric minerals nontronite (905–940 nm), goethite (890–910 nm), and jarosite (880–910 nm), in addition to the ferrous silicate orthopyroxene (890–920 nm). Akaganeite band centers are typically below this range (870–880 nm), and both goethite and akaganeite are likely ruled out based on the association between >900 nm band centers and weaker 527 nm absorptions discussed above (Figure S6 in Supporting Information S1). At the Sebina drill site, the only drill sample collected in the Sutton Island member, goethite and akaganeite were not detected, and jarosite was detected at <1% (Rampe et al., 2020).

In contrast, nontronite is the only candidate mineral here that is known to encompass the whole range of longer wavelength band centers observed in Sutton Island (Figure S4 in Supporting Information S1), that is present in the Duluth drill sample in Blunts Point (McAdam et al., 2020), and that has also been detected from orbital data (Carter et al., 2016). Phyllosilicates are common in the Murray formation (detected at ~20% in Sebina from CheMin; Rampe et al., 2020), but are likely masked in most Mastcam spectra by fine-grained crystalline hematite. In Mastcam spectra of several drilled sites in lower Glen Torridon, where hematite was found in small quantities (<1–4 wt.%) but phyllosilicates were abundant (up to 34 wt. %), band centers are shifted toward longer wavelengths and ChemCam passive spectra (Johnson et al., 2019) of these targets exhibit a flattening at ~650 nm, consistent with Fe/Mg-smectites (Rudolph et al., 2022). The spectral similarities between SI and lower

Glen Torridon are consistent with APXS data which show that these regions have the greatest overlap in bedrock chemistry within the Murray (Rudolph et al., 2022).

Comparing band center and band depth with chemistry can help determine which minerals are causing the shift in band center to long wavelengths. No significant relationship was observed between location of the >900 nm band center and chemostratigraphy of sulfur or chlorine, which would have suggested a change in jarosite or akaganeite content respectively. However, we did see changes in band center trending with increased Li and CIA, both of which have been shown to be related to increases in clay mineral content in terrestrial rocks (Frydenvang et al., 2020; Mangold et al., 2019; Nesbitt & Young, 1982). Li and CIA increase through Sutton Island and Blunts Point before decreasing in VRR and trending upwards again in clay mineral rich Glen Torridon (Figure S2 in Supporting Information S1; Frydenvang et al., 2020).

Due to the pigmentary nature of crystalline fine-grained hematite, which would dominate spectra in even very small quantities (Figure S5; Cornell & Schwertmann, 2003), band centers greater than ~900 nm imply that there is no more than ~3 wt.% fine grained crystalline hematite in the mixture, which is consistent with results from Mastcam and CheMin in Glen Torridon (Rudolph et al., 2022). The patchiness of absorption features centered at ~867 nm in the bedrock of Sutton Island relative to bedrock in other parts of the Murray Formation points to a lack of crystalline fine-grained hematite in parts of this region. While the second class of spectra observed here (Figure 4) are non-unique, nontronite is most consistent with the properties of the spectra, including the longer wavelength band center (905–940 nm), and this interpretation is supported by the chemical trends stated above along with other evidence for increased clay content in this region.

It is likely that phyllosilicates are present throughout Sutton Island, and potentially at higher abundances than most other locations in the Murray formation. Even where hematite bands dominate, these bands usually appear deeper than neighboring parts of the Murray, as indicated by trends in BD867 (Figure 9; Fraeman, Edgar, et al., 2020; Fraeman, Johnson, et al., 2020; Rice et al., 2022). This deepening of the hematite band is consistent with increased clay mineral content in this region, as even small amounts of ferric phyllosilicates have been found to increase BD867 values in lab mixtures (Jacob et al., 2020). Alternatively, deeper hematite bands could also be due to greater crystallinity of the hematite in Sutton Island, as hypothesized for the strongest hematite bands observed on VRR (Fraeman, Edgar, et al., 2020; Fraeman, Johnson, et al., 2020; Horgan et al., 2020).

The spectra in Class 3, which have been observed in the dark gray features in Sutton Island (Figure 5), do not exhibit the long wavelength absorption bands associated with the bedrock spectra in this study. This feature occurs in fracture fills and diagenetic concretions and is therefore likely an alteration mineral, such as a coarse-grained Fe-oxide (e.g., hematite or magnetite; Figure 3). The blue slope toward 1,000 nm could be due to either a blue slope extending beyond 1,000 nm, consistent with very fine grained or glassy basalts (e.g., Farrand & Singer, 1992; Henderson et al., 2021), or more likely a broad iron absorption band centered at or beyond 1,000 nm, as observed in minerals like olivine, high-Ca pyroxene, and mixed valence Fe-bearing phyllosilicates. Similar flat and/or blue sloped spectra have been observed in association with dark diagenetic features in Vera Rubin ridge, where it was interpreted as due to coarse-grained hematite (Horgan et al., 2020; L'Haridon et al., 2020).

In general, dark diagenetic features in this region are spectrally variable and we did not observe any significant correlations or trends between feature morphology, color, or size and Mastcam spectral parameters. While the spectra in Class 3 appear to be exclusive to diagenetic features, not all dark diagenetic features in Sutton Island exhibit this type of spectra, as they often also exhibit spectra consistent with hematite or Fe/Mg-clays (e.g., Figure 6a), much like the local bedrock. However, it should be noted that diagenetic features are often small and therefore difficult to draw large enough ROI's that we can collect accurate spectra from, and few are visible in Mastcam multispectral images in this member, so our dataset may be biased toward the largest examples.

5. Discussion

The Sutton Island member's distinctive spectral properties suggest it has a different mineralogy than the underlying Murray. Specifically, while absorptions at 530 and 860 nm show crystalline fine-grained hematite is present in most of the Mastcam spectra below Glen Torridon, elsewhere in neighboring regions of the Murray, these absorptions are only present in localized patches in Sutton Island. Instead, much of the bedrock spectra in Sutton Island are associated with spectral absorptions at ~900 nm or longer. Mastcam images show that Sutton Island

also exhibits unique and abundant diagenetic features. Together, these observations suggest that Sutton Island experienced a unique aqueous alteration history compared to the rest of the Murray, and here we investigate possible depositional and diagenetic scenarios.

5.1. Deposition and Early Diagenesis of Sutton Island Sediments

We hypothesize that the Sutton Island member was deposited in a lakeshore or low stand setting. A lakeshore environment with significant fluvial input is supported by the presence of heterolithic fluvial and lacustrine facies in Sutton Island (Fedo et al., 2018), and the presence of desiccation cracks, such as on Old Soaker, is indicative of increased subaerial exposure (Stein et al., 2018). Additionally, the bedrock sulfate enrichment observed by ChemCam in discrete beds of heterolithic facies (Rapin et al., 2019) in this region suggests deposition along a shallow and evaporative lake margin, rather than a deeper lacustrine setting like the rest of the Murray. Hydrous Fe and Mn-oxides found in Sutton Island are often formed closer to the shoreline of marine and lacustrine environments (Meslin et al., 2018).

We also hypothesize that rocks in the Sutton Island member experienced sub-aerial exposure and weathering. Sub-aerial weathering in an open-system would have formed dioctahedral clays, such as nontronite, in this region, and therefore Sutton Island may represent the best record encountered by MSL of surface conditions on the margin and beyond the ancient lakes in Gale during deposition of the lacustrine Murray formation. While similar spectra that are consistent with clays are visible in lower Glen Torridon (Rudolph et al., 2022), the lack of sedimentological evidence of surface exposure, such as desiccation cracks, suggests that clays in Glen Torridon are authigenic and formed through lacustrine processes.

The presence of abundant clay minerals in Sutton Island may have limited penetration of diagenetic fluids in this area due to their lower permeability (Frydenvang et al., 2020; Kamann et al., 2007). On Earth, clay minerals exhibit varying levels of porosity and permeability in bedrock depending on whether they are coating grain surfaces or filling pore spaces (Worden & Morad, 1999). Similar relatively low permeabilities due to abundant clay minerals preventing later diagenesis have also been proposed for the most smectite-rich parts of Glen Torridon (Rudolph et al., 2022).

Hematite is present throughout the Murray where the bedrock interacted with oxidizing diagenetic fluids (Horgan et al., 2020; Hurowitz et al., 2017; Rampe et al., 2017) and/or silica poor brines (Bristow et al., 2021). We hypothesize that hematite is overall less abundant in Sutton Island compared to the rest of the Murray below Glen Torridon because the sediments did not interact with the same oxidizing fluids. Additionally, the lack of hematite associated with postulated surface weathering suggests that the atmosphere was not the primary source of oxidants and that oxidation instead occurred in the lake waters or due to diagenetic fluids. This could be due to a less oxidizing atmosphere or the low permeability of sediments creating a more closed and reducing system.

Alternatively, fine grained crystalline hematite could be absent in much of Sutton Island because it formed initially and was later removed, for example, by diagenetic fluids that remobilized and removed the hematite in parts of Sutton Island. Dissolution of fine-grained red hematite by reducing or acidic diagenetic fluids has been proposed to have created bleached zones on VRR and in Glen Torridon (Horgan et al., 2020; Rudolph et al., 2022). However, bedrock color variations in Sutton Island are less widespread and light toned bedrock does not exhibit the same spectral characteristics as it does on VRR and in Glen Torridon. In addition, in these other areas where hematite dissolution has been proposed, the fluids are thought to have destroyed clay minerals as well (Rampe et al., 2020; Rudolph et al., 2022), which is inconsistent with their apparent persistence in Sutton Island in Mastcam data, and suggests that those fluids never penetrated into Sutton Island bedrock. Finally, as discussed below, the morphology and distribution of diagenetic features of Sutton Island is more consistent with limited flow of late diagenetic fluids, making it less likely that late diagenesis preferentially removed hematite in Sutton Island compared to surrounding intervals.

5.2. Late Diagenesis of Sutton Island

The diagenetic features of Sutton Island are consistent with those observed in low permeability bedrock on Earth. As diagenetic fluids cannot move easily through parts of less permeable rocks, they tend to cause spatially heterogeneous alteration. Mudstones have far more variability in porosity, composition, bedding styles, and fabrics than

other rocks (Macquaker et al., 2014) and all of these can affect the movement of diagenetic fluids. Mudstones are also susceptible to compaction which can reduce permeability and pore space (Dowey & Taylor, 2020). Heterogeneities within rocks will cause fluids to concentrate in more porous and permeable parts of an outcrop such as fractures and between bedding planes.

Dark flat features interbedded in outcrops and mottled dark toned surfaces covering an entire outcrop may be evidence of alteration along fractures and fracture fills, respectively (Figure 2), which must form late, after lithification. Heterogeneities within rocks will cause fluids to concentrate in more porous and permeable parts of an outcrop such as fractures and between bedding planes (Potter-McIntyre et al., 2014). For example, the dark toned mottled feature that covers nearly the entire outcrop of Parker Bog could be the remnant of a fracture fill formed by late-stage diagenetic fluids (Figure 7). Flat concretions that preserve primary host rock laminae may have infiltrated along more permeable bedding planes during late diagenesis (Sun et al., 2019) or formed during early diagenesis in an oxidizing lowstand or nearshore environment (Meslin et al., 2018). These features are much more common in Sutton Island and Blunts Point than elsewhere in the Murray.

We hypothesize that increased clay mineral content and heterogeneous grain size in this region caused an increase in diagenetic features with irregular morphologies and that the bedrock in Sutton Island and Blunts Point was exposed to several different diagenetic fronts during multiple episodes of diagenesis.

While dark features in Sutton Island exhibit a variety of morphologies, there is no significant relationship found between their morphology and spectral properties. Many of the spectra observed in dark features show peaks at shorter wavelengths, ~690–750 nm, which are less common in bedrock (Figure 5). Clear diagenetic context suggests this is not due to primary mafic minerals like olivine, but instead is potentially consistent with magnetite or coarse-grained varieties of other iron oxides. Some of the dark features exhibit significant local variability in their spectra, such as the Parker Bog outcrop (Figure 7), which displays both fine-grained crystalline hematite-like spectra and spectra with peaks at shorter wavelengths, possibly suggesting a mix of coarse- and fine-grained iron oxides, hematite and possibly magnetite, that may be evidence of multiple stages of diagenetic fluids with variable chemistry and/or redox states. Concretions, nodules, and other dark diagenetic features within bedrock are variable in a similar manner, and often also resemble local bedrock implying that they were formed through the cementation or recrystallization of local materials.

Almost all of these dark features show enhanced Fe and Mn, consistent with enrichment of iron oxides, and many have enhanced P, which is most strongly associated with Fe-rich targets. These enrichments point to highly oxidizing conditions at the water-sediment interface likely in a near-surface environment (Meslin et al., 2018). The morphologies of these enrichments are similar to phosphorite fabrics on earth that form from the reworking of laminae in a more shallow lacustrine environment (Meslin et al., 2018). The varying chemistry and morphology of these features implies that they were formed from several different episodes of diagenetic fluid flow (Sun et al., 2019).

5.3. Implications

Understanding the formation and alteration of the Sutton Island member is important to better constrain paleo-lake Gale and the timing and chemistry of diagenetic fluids. This region has some of the best evidence so far of a low stand or lake margin environment that experienced sub-aerial weathering (Fedo et al., 2018; Meslin et al., 2018; Rivera-Hernandez et al., 2020; Stein et al., 2018). In terrestrial weathering profiles, increased alteration and weathering is associated with increasing dioctahedral clay content (e.g., Chamley, 1989) and increased CIA (Nesbitt & Young, 1982), both of which are consistent with observations from CheMin (Bristow et al., 2018) and ChemCam (Mangold et al., 2019). This departure from the sustained lacustrine depositional environment that some other parts of the Murray preserve suggests a reduction in the hydrological budget in this area, groundwater availability, or an overall trend in global desiccation (Rapin et al., 2019). However, the persistence of weathering in the near-shore environment suggests that the climate was not completely arid, as SMECTITE formation on Earth typically occurs under semi-arid (mean annual precipitation ~200–1,000 mm/year), temperate to warm, and often strongly seasonal conditions (e.g., Graham & O'Geen, 2010; Singer, 1980). Understanding these low stand environments in closed-basin lakes is also important for the search for biosignatures, as they provide a unique ecological niche for organisms like photosynthetic microbes. Curiosity may encounter more records of

sub-aerial or shallow lake environments further up Mt. Sharp as the rover approaches another interval of sulfate enriched bedrock (Rapin et al., 2021).

Understanding diagenetic history is crucial for gaining insight into habitability in Gale because diagenetic fluids can overprint authigenic mineral records that provide key constraints on the timing and types of environments that existed. In Sutton Island, the presence of clay minerals appears to have decreased permeability of the sediments, thereby driving significant spatial variability in diagenetic alteration. Similar relationships have been observed on VRR, where clay mineral abundances appear to be correlated with the preservation of early diagenetic features (Rudolph et al., 2022). The decreased permeability of bedrock enriched with clay minerals thus also allows for increased biosignature preservation potential (e.g., Summons et al., 2011; Velde, 1995; Wattel-Koekkoek & Buurman, 2004). For example, diagenetic fluid interactions with sediments that likely caused the cementation and recrystallization on the Vera Rubin ridge (Fraeman, Edgar, et al., 2020; Fraeman, Johnson, et al., 2020; Horgan et al., 2020; L'Haridon et al., 2020) could break down organics and biosignatures (Hays et al., 2017), while sulfurization during early diagenesis likely contributed to the preservation of organics elsewhere in Gale (Eigenbrode et al., 2018).

6. Conclusions

In Mastcam spectra, most bedrock in the Sutton Island member lacks the spectral absorptions attributed to hematite found throughout the Murray formation and instead display deeper absorption bands shifted to longer wavelengths that are consistent with Fe-bearing smectites like nontronite (Figure 9). These spectral signatures occur in a region with increased Li and Chemical Index of Alteration (CIA) (Figure S2 in Supporting Information S1), both of which could also be related to an increase in clay mineral content. Combined, these observations suggest that the Sutton Island member has a distinct mineralogy compared to the rest of the Murray formation. We propose the Sutton Island bedrock contains less crystalline hematite and more Fe-smectites, such as nontronite, compared to surrounding regions.

We propose that Sutton Island contains more smectites due to surface weathering during a low stand along an ancient lake shoreline within Gale crater, as supported by the presence of desiccation features, and the decrease in the water availability during this time period may have been caused by larger climatic changes. Sutton Island also exhibits diagenetic features with textures and spectral properties (dark concretions, dark fracture fills, and bedrock color variations) that are not present or less common elsewhere in the Murray formation (Sun et al., 2019). Increased clay mineral abundances and heterogeneity in grain size could have produced relatively impermeable zones within Sutton Island, which would have inhibited diagenetic fluid flow in certain areas, resulting in the varied diagenetic alteration observed in this area (e.g., possible bleaching, large dark fracture fills, and dark mottling). Diagenetic fluids greatly affect the preservation of biosignatures and clay rich rocks generally have a very high biosignature preservation potential (e.g., Summons et al., 2011; Velde, 1995; Wattel-Koekkoek & Buurman, 2004).

As MSL continues to ascend Mt. Sharp, we may see similar facies within sulfate bearing strata which were likely deposited in a more arid climate than the lower Murray formation (Rapin et al., 2021), reflecting a global climatic change (Bibring et al., 2007; Grotzinger et al., 2012). The results of this study show that Sutton Island may be important to understanding this transition and our findings will help future missions to identify similar regions of interest with rover and orbital data.

Data Availability Statement

All Mastcam (Malin, 2013) and MAHLI (Edgett, 2013) images in this manuscript are publicly available on the Planetary Data System (PDS) Geosciences Node (<https://pds-imaging.jpl.nasa.gov/volumes/msl.html>) in addition to HiRISE images (McEwen, 2007; <https://pds-imaging.jpl.nasa.gov/volumes/mro.html>). All ChemCam passive spectra (Johnson & Ward, 2022), LIBS data (Wiens, 2013; <https://pds-geosciences.wustl.edu/missions/msl/chemcam.htm>), and APXS data (Gellert, 2012; <https://pds-geosciences.wustl.edu/missions/msl/apxs.htm>) are also freely available on the PDS. Mastcam spectra collected in this study are available on Mendeley (Haber, 2022).

Acknowledgments

We thank the MSL science and operations teams for their tireless work in collecting, processing, and compiling all the data used in this study. We would also like to thank William Farrand and an anonymous reviewer for their thorough revisions which improved this manuscript's clarity and coherence. This work was supported by the NASA Mars Science Laboratory Participating Scientist Program and the Purdue University Department of Earth, Atmospheric, and Planetary Sciences. EAC thanks the Natural Sciences and Engineering Research Council of Canada and the Canadian Space Agency for their support. We would also like to acknowledge Amanda Rudolph for her feedback concerning Glen Torridon and Mason Starr for sharing Mastcam spectra collected at Western Washington University.

References

- Anderson, R. B., & Bell, J. F. (2013). Correlating multispectral imaging and compositional data from the Mars Exploration Rovers and implications for Mars Science Laboratory. *Icarus*, 223(1), 157–180. <https://doi.org/10.1016/j.icarus.2012.11.029>
- Banham, S. G., Gupta, S., Rubin, D. M., Watkins, J. A., Sumner, D. Y., Edgett, K. S., et al. (2018). Ancient Martian aeolian processes and palaeomorphology reconstructed from the Stimson formation on the lower slope of Aeolis Mons, Gale crater, Mars. *Sedimentology*, 65(4), 993–1042. <https://doi.org/10.1111/sed.12469>
- Bell, J. F., Godber, A., McNair, S., Caplinger, M. A., Maki, J. N., Lemmon, M. T., et al. (2017). The Mars Science Laboratory Curiosity rover Mastcam instruments: Preflight and in-flight calibration, validation, and data archiving. *Earth and Space Science*, 4(7), 396–452. <https://doi.org/10.1002/2016ea000219>
- Berger, J. A., Gellert, R., Boyd, N. I., King, P. L., McCraig, M. A., O'Connell-Cooper, C. D., et al. (2020). Elemental composition and chemical evolution of geologic materials in Gale crater, Mars: APXS results from Bradbury landing to the Vera Rubin Ridge. *Journal of Geophysical Research: Planets*, 125(12). <https://doi.org/10.1029/2020je006536>
- Bibring, J.-P., Arvidson, R. E., Gendrin, A., Gondet, B., Langevin, Y., Mouelic, S. L., et al. (2007). Coupled ferric oxides and sulfates on the Martian surface. *Science*, 317(5842), 1206–1210. <https://doi.org/10.1126/science.1144174>
- Blake, D., Vaniman, D., Achilles, C., Anderson, R., Bish, D., Bristow, T., et al. (2012). Characterization and calibration of the CheMin mineralogical instrument on Mars Science Laboratory. *Space Science Reviews*, 170(1–4), 341–399. <https://doi.org/10.1007/s11214-012-9905-1>
- Bristow, T. F., Grotzinger, J. P., Rampe, E. B., Cuadros, J., Chipera, S. J., Downs, G. W., et al. (2021). Brine-driven destruction of clay minerals in Gale crater, Mars. *Science (New York, N.Y.)*, 373(6551), 198–204. <https://doi.org/10.1126/science.abg5449>
- Bristow, T. F., Rampe, E. B., Achilles, C. N., Blake, D. F., Chipera, S. J., Craig, P., et al. (2018). Clay mineral diversity and abundance in sedimentary rocks of Gale crater, Mars. *Science Advances*, 4(6), eaar3330. <https://doi.org/10.1126/sciadv.aar3330>
- Campbell, J. L., Perrett, G. M., Gellert, R., Andrushenko, S. M., Boyd, N. I., Maxwell, J. A., et al. (2012). Calibration of the Mars Science Laboratory Alpha particle X-ray spectrometer. *Space Science Reviews*, 170(1–4), 319–340. <https://doi.org/10.1007/s11214-012-9873-5>
- Carter, J., Quantin, C., Thollot, P., Loizeau, D., Ody, A., & Lozach, L. (2016). Oxia Planum: A clay-Laden Landing site proposed for the ExoMars rover mission: Aqueous mineralogy and alteration scenarios, Lunar and Planetary science conference #2064.
- Catalano, J. G. (2013). Thermodynamic and mass balance constraints on iron-bearing phyllosilicate formation and alteration pathways on early Mars. *Journal of Geophysical Research: Planets*, 118(10), 2124–2136. <https://doi.org/10.1002/jgre.20161>
- Chamley, H. (1989). Clay minerals. *Clay Sedimentology*, 3–20. https://doi.org/10.1007/978-3-642-85916-8_1
- Chemtob, S. M., Nickerson, R. D., Morris, R. V., Agresti, D. G., & Catalano, J. G. (2017). Oxidative alteration of ferrous smectites and implications for the redox evolution of early Mars. *Journal of Geophysical Research: Planets*, 122(12), 2469–2488. <https://doi.org/10.1002/2017je005331>
- Clark, R. N., Swayze, G. A., Wise, R. A., Livo, K. E., Hoefen, T. M., Kokaly, R. F., & Sutley, S. J. (2007). *USGS digital spectral library SPLIB06A (No. 231)*. US Geological Survey.
- Clegg, S. M., Wiens, R. C., Anderson, R., Forni, O., Frydenvang, J., Lasue, J., et al. (2017). Recalibration of the Mars Science Laboratory ChemCam instrument with an expanded geochemical database. *Spectrochimica Acta Part B: Atomic Spectroscopy*, 129, 64–85. <https://doi.org/10.1016/j.sab.2016.12.003>
- Cloutis, E. A., Hawthorne, F. C., Mertzman, S. A., Krenn, K., Craig, M. A., Marcino, D., et al. (2006). Detection and discrimination of sulfate minerals using reflectance spectroscopy. *Icarus*, 184(1), 121–157. <https://doi.org/10.1016/j.icarus.2006.04.003>
- Cornell, R. M., & Schwertmann, U. (2003). The iron oxides. <https://doi.org/10.1002/3527602097>
- Dowey, P. J., & Taylor, K. G. (2020). Diagenetic mineral development within the upper Jurassic Haynesville-Bossier shale, USA. *Sedimentology*, 67(1), 47–77. <https://doi.org/10.1111/sed.12624>
- Edgar, L. A., Fedo, C. M., Gupta, S., Banham, S. G., Fraeman, A. A., Grotzinger, J. P., et al. (2020). A lacustrine paleoenvironment recorded at Vera Rubin Ridge, Gale crater: Overview of the sedimentology and stratigraphy observed by the Mars Science Laboratory Curiosity rover. *Journal of Geophysical Research: Planets*, 125(3). <https://doi.org/10.1029/2019je006307>
- Edgett, K. (2013). MSL Mars Hand Lens imager camera RDR V1.0, NASA Planetary data system. <https://doi.org/10.17189/1520292>
- Eigenbrode, J. L., Summons, R. E., Steele, A., Freissinet, C., Millan, M., Navarro-González, R., et al. (2018). Organic matter preserved in 3-billion-year-old mudstones at Gale crater, Mars. *Science*, 360(6393), 1096–1101. <https://doi.org/10.1126/science.aas9185>
- Farrand, W. H., Bell, J. F., III, Johnson, J. R., Joliff, B. L., Knoll, A. H., McLennan, S. M., et al. (2007). Visible and near-infrared multispectral analysis of rocks at Meridiani Planum, Mars by the Mars exploration rover opportunity. *Journal of Geophysical Research*, 112(E6), E06S02. <https://doi.org/10.1029/2006JE002773>
- Farrand, W. H., Johnson, J. R., Rice, M. S., Wang, A., & Bell, J. F., III. (2016). VNIR multispectral observations of aqueous alteration materials by the Pancams on the spirit and opportunity Mars Exploration Rovers. *American Mineralogist*, 101(9), 2005–2019. <https://doi.org/10.2138/am-2016-5627>
- Farrand, W. H., & Singer, R. B. (1992). Alteration of hydrovolcanic basaltic ash: Observations with visible and near-infrared spectrometry. *Journal of Geophysical Research*, 97(B12), 17393–17408. <https://doi.org/10.1029/92jb01075>
- Fedo, C. M., Grotzinger, J. P., Gupta, S., Banham, S., Bennett, K., Edgar, L., et al. (2019). Evidence for persistent, water-rich, lacustrine deposition preserved in the Murray formation, Gale crater: A depositional system suitable for sustained habitability. *Paper presented at ninth international conference on Mars*. 6308.
- Fedo, C. M., Grotzinger, J. P., Fraeman, A., Edgar, L., Edgett, K., et al. (2018). Sedimentology and stratigraphy of the Murray formation, Gale crater, Mars. In *The 49th lunar and planetary science conference*. 2078
- Fedo, C. M., Nesbitt, H. W., & Young, G. M. (1995). Unraveling the effects of potassium metasomatism in sedimentary rocks and paleosols, with implications for paleoweathering conditions and provenance. *Geology*, 23(10), 921–924. [https://doi.org/10.1130/0091-7613\(1995\)023<0921:uteopm>2.3.co;2](https://doi.org/10.1130/0091-7613(1995)023<0921:uteopm>2.3.co;2)
- Forni, O., Gaft, M., Toplis, M. J., Clegg, S. M., Maurice, S., Wiens, R. C., et al. (2015). First detection of fluorine on Mars: Implications for Gale crater's geochemistry. *Geophysical Research Letters*, 42(4), 1020–1028. <https://doi.org/10.1002/2014gl062742>
- Forni, O., Nachon, M., Mangold, N., Blaney, D. L., Wiens, R. C., Clegg, S. M., et al. (2016). *Fluorine in the Pahrump outcrop, Gale crater: Implications for fluid circulation and alteration*, LPS XLVII. Abstract 1990.
- Fraeman, A. A., Edgar, L. A., Rampe, E. B., Thompson, L. M., Frydenvang, J., Fedo, C. M., et al. (2020). Evidence for a diagenetic origin of Vera Rubin Ridge, Gale crater, Mars: Summary and synthesis of Curiosity's exploration campaign. *Journal of Geophysical Research: Planets*, 125(12), e2020JE006527. <https://doi.org/10.1029/2020je006527>
- Fraeman, A. A., Ehlmann, B. L., Arvidson, R. E., Edwards, C. S., Grotzinger, J. P., Milliken, R. E., et al. (2016). The stratigraphy and evolution of lower Mount Sharp from spectral, morphological, and thermophysical orbital data sets. *Journal of Geophysical Research: Planets*, 121(9), 1713–1736. <https://doi.org/10.1002/2016je005095>

- Fraeman, A. A., Johnson, J. R., Arvidson, R. E., Rice, M. S., Wellington, D. F., Morris, R. V., et al. (2020). Synergistic ground and orbital observations of iron oxides on Mt. Sharp and Vera Rubin Ridge. *Journal of Geophysical Research: Planets*, 125(9), e2019JE006294. <https://doi.org/10.1029/2019je006294>
- Frydenvang, J., Gasda, P. J., Hurowitz, J. A., Grotzinger, J. P., Wiens, R. C., Newsom, H. E., et al. (2017). Diagenetic silica enrichment and late-stage groundwater activity in Gale crater, Mars. *Geophysical Research Letters*, 44(10), 4716–4724. <https://doi.org/10.1002/2017gl073323>
- Frydenvang, J., Mangold, N., Wiens, R. C., Fraeman, A. A., Edgar, L. A., Fedo, C. M., et al. (2020). The chemostratigraphy of the Murray formation and role of diagenesis at Vera Rubin ridge in Gale crater, Mars, as observed by the ChemCam instrument. *Journal of Geophysical Research: Planets*, 125(9). <https://doi.org/10.1029/2019je006320>
- Gasda, P. ~J., Lanza, N., Meslin, P.-Y., Forni, O., L'Haridon, J., Fischer, W. ~W., et al. (2019). High-Mn sandstone as evidence for oxidized conditions in Gale crater lake, 1620.
- Gellert, R. (2012). MSL Mars alpha particle X-ray spectrometer 2 EDR V1.0 [Dataset]. NASA Planetary Data System, <https://doi.org/10.17189/1519534>
- Gillespie, A. R., Kahle, A. B., & Walker, R. E. (1986). Color enhancement of highly correlated images. I. Decorrelation and HSI contrast stretches. *Remote Sensing of Environment*, 20(3), 209–235. [https://doi.org/10.1016/0034-4257\(86\)90044-1](https://doi.org/10.1016/0034-4257(86)90044-1)
- Graham, R. C., & O'Geen, A. T. (2010). Soil mineralogy trends in California landscapes. *Geoderma*, 154(3–4), 418–437. <https://doi.org/10.1016/j.geoderma.2009.05.018>
- Grotzinger, J. P., Crisp, J., Vasavada, A. R., Anderson, R. C., Baker, C. J., Barry, R., et al. (2012). Mars Science Laboratory mission and science investigation. *Space Science Reviews*, 170(1–4), 5–56. <https://doi.org/10.1007/s11214-012-9892-2>
- Grotzinger, J. P., Gupta, S., Malin, M. C., Rubin, D. M., Schieber, J., Siebach, K., et al. (2015). Deposition, exhumation, and paleoclimate of an ancient lake deposit, Gale crater, Mars. *Science*, 350(6257), aac7575. <https://doi.org/10.1126/science.aac7575>
- Grotzinger, J. P., Sumner, D. Y., Kah, L. C., Stack, K., Gupta, S., Edgar, L., et al. (2014). A habitable fluvio-lacustrine environment at Yellowknife Bay, Gale crater, Mars. *Science*, 343(6169), 1242777. <https://doi.org/10.1126/science.1242777>
- Gwizd, S., Fedo, C., Grotzinger, J., Edgett, K., Gupta, S., Stack, K. M., et al. (2019). Toward a greater understanding of facies in the Hartmann's valley member of the Murray formation, Gale crater, Mars. In *The ninth international conference on Mars*. 6183.
- Haber, J. (2022). Data for: Mineralogy of a possible ancient lakeshore in the Sutton Island member of Mt. Sharp, Gale crater, Mars, from Mastcam multispectral images. *Mendeley Data*, V1, e2021JE007134. <https://doi.org/10.17632/xmpnfd79bt.1>
- Hays, L. E., Graham, H. V., Marais, D. J. D., Hausrath, E. M., Horgan, B., McCollom, T. M., et al. (2017). Biosignature preservation and detection in Mars analog environments. *Astrobiology*, 17(4), 363–400. <https://doi.org/10.1089/ast.2016.1627>
- Henderson, M. J. B., Horgan, B. H. N., Rowe, M. C., Wall, K. T., & Scudder, N. A. (2021). Determining the volcanic eruption style of Tephra deposits from infrared spectroscopy. *Earth and Space Science*, 8(2). <https://doi.org/10.1029/2019ea001013>
- Horgan, B. H. N., Johnson, J. R., Fraeman, A. A., Rice, M. S., Seeger, C., Bell, J. F., et al. (2020). Diagenesis of Vera Rubin Ridge, Gale crater, Mars, from Mastcam multispectral images. *Journal of Geophysical Research: Planets*, 125(11), e2019JE006322. <https://doi.org/10.1029/2019je006322>
- Hurowitz, J. A., Grotzinger, J. P., Fischer, W. W., McLennan, S. M., Milliken, R. E., Stein, N., et al. (2017). Redox stratification of an ancient lake in Gale crater, Mars. *Science*, 356(6341). <https://doi.org/10.1126/science.aah6849>
- Jacob, S. R., Wellington, D. F., Bell, J. F., Achilles, C., Fraeman, A. A., Horgan, B., et al. (2020). Spectral, compositional, and physical properties of the upper Murray formation and Vera Rubin Ridge, Gale crater, Mars. *Journal of Geophysical Research: Planets*, 125(11), e2019JE006290. <https://doi.org/10.1029/2019je006290>
- Johnson, J. R., Bell, J. F., Bender, S., Blaney, D., Cloutis, E., DeFlores, L., et al. (2015). ChemCam passive reflectance spectroscopy of surface materials at the curiosity landing site, Mars. *Icarus*, 249, 74–92. <https://doi.org/10.1016/j.icarus.2014.02.028>
- Johnson, J. R., Bell, J. F., Bender, S., Blaney, D., Cloutis, E., Ehlmann, B., et al. (2016). Constraints on iron sulfate and iron oxide mineralogy from ChemCam visible/near-infrared reflectance spectroscopy of Mt. Sharp basal units, Gale Crater, Mars. *American Mineralogist*, 101(7), 1501–1514. <https://doi.org/10.2138/am-2016-5553>
- Johnson, J. R., Fraeman, A., Horgan, B. H. N., Rice, M. S., Wiens, R. C., & Maurice, S. (2019). *ChemCam visible/near-infrared spectra of drill tailings and nontronite-bearing rocks in the northern Glen Torridon area, Gale crater, Mars*, 2019. AGU Fall Meeting. 489891.
- Johnson, J. R., & Ward, J. (2022). MSL ChemCam passive surface spectra bundle, NASA 1167 Planetary data system. <https://doi.org/10.17189/1520577>
- Kamann, P. J., Ritz, R. W., Dominic, D. F., & Conrad, C. M. (2007). Porosity and permeability in sediment mixtures. *Ground Water*, 45(4), 429–438. <https://doi.org/10.1111/j.1745-6584.2007.00313.x>
- Kronyak, R. E., Kah, L. C., Edgett, K. S., Van Bommel, S. J., Thompson, L. M., Wiens, R. C., et al. (2019). Mineral-filled fractures as indicators of Multigenerational fluid flow in the Pahrump Hills member of the Murray formation, Gale crater, Mars. *Earth and Space Science*, 6(2), 238–265. <https://doi.org/10.1029/2018ea000482>
- L'Haridon, J., Mangold, N., Fraeman, A. A., Johnson, J. R., Cousin, A., Rapin, W., et al. (2020). Iron Mobility during diagenesis at Vera Rubin Ridge, Gale crater, Mars. *Journal of Geophysical Research: Planets*, 125(11). <https://doi.org/10.1029/2019je006299>
- Macquaker, J. H. S., Taylor, K. G., Keller, M., & Poly, D. (2014). Compositional controls on early diagenetic pathways in fine-grained sedimentary rocks: Implications for predicting unconventional reservoir attributes of mudstones. *AAPG Bulletin*, 98(3), 587–603. <https://doi.org/10.1306/08201311176>
- Malin, M. (2013). MSL Mars mast camera RDR V1.0, NASA Planetary data system. <https://doi.org/10.17189/1520328>
- Malin, M. C., Ravine, M. A., Caplinger, M. A., Ghaemi, F. T., Schaffner, J. A., Maki, J. N., et al. (2017). The Mars Science Laboratory (MSL) Mast cameras and Descent imager: Investigation and instrument descriptions. *Earth and Space Science*, 4(8), 506–539. <https://doi.org/10.1002/2016ea000252>
- Mangold, N., Dehouck, E., Fedo, C., Forni, O., Achilles, C., Bristow, T., et al. (2019). Chemical alteration of fine-grained sedimentary rocks at Gale crater. *Icarus*, 321, 619–631. <https://doi.org/10.1016/j.icarus.2018.11.004>
- Maurice, S., Wiens, R. C., Saccoccio, M., Barraclough, B., Gasnault, O., Forni, O., et al. (2012). The ChemCam instrument suite on the Mars Science Laboratory (MSL) rover: Science objectives and mast unit description. *Space Science Reviews*, 170(1–4), 95–166. <https://doi.org/10.1007/s11214-012-9912-2>
- McAdam, A. C., Sutter, B., Archer, P. D., Franz, H. B., Wong, G. M., Lewis, J. M. T., et al. (2020). Constraints on the mineralogy and geochemistry of Vera Rubin Ridge, Gale crater, Mars, from Mars Science Laboratory sample analysis at Mars evolved gas analyses. *Journal of Geophysical Research: Planets*, 125(11). <https://doi.org/10.1029/2019je006309>
- McEwen, A. (2007). Mars Reconnaissance orbiter high resolution imaging science experiment, reduced data record, MRO-M-HIRISE-3-RDR-V1.1. NASA Planetary Data System. <https://doi.org/10.17189/1520303>

- Meslin, P. Y., Gasda, P., L'Haridon, J., Forni, O., Lanza, N., Lamm, S., et al. (2018). Detection of hydrous manganese and iron oxides with variable phosphorus and magnesium contents in the lacustrine sediments of the Murray formation, Gale, Mars. In *The 49th lunar and planetary science conference*. Abstract #1447.
- Milliken, R. E., Grotzinger, J. P., & Thomson, B. J. (2010). Paleoclimate of Mars as captured by the stratigraphic record in Gale Crater. *Geophysical Research Letters*, 37(4). <https://doi.org/10.1029/2009gl041870>
- Morris, R. V., Lauer, H. V., Lawson, C. A., Gibson, E. K., Nace, G. A., & Stewart, C. (1985). Spectral and other physicochemical properties of submicron powders of hematite (α -Fe₂O₃), maghemite (γ -Fe₂O₃), magnetite (Fe₃O₄), goethite (α -FeOOH), and lepidocrocite (γ -FeOOH). *Journal of Geophysical Research*, 90(B4), 3126–3144. <https://doi.org/10.1029/jb090ib04p03126>
- Nachon, M., Clegg, S. M., Mangold, N., Schröder, S., Kah, L. C., Dromart, G., et al. (2014). Calcium sulfate veins characterized by ChemCam/Curiosity at Gale crater, Mars. *Journal of Geophysical Research: Planets*, 119(9), 1991–2016. <https://doi.org/10.1002/2013je004588>
- Nachon, M., Mangold, N., Forni, O., Kah, L. C., Cousin, A., Wiens, R. C., et al. (2017). Chemistry of diagenetic features analyzed by ChemCam at Pahrump Hills, Gale crater, Mars. *Icarus*, 281, 121–136. <https://doi.org/10.1016/j.icarus.2016.08.026>
- Nesbitt, H. W., & Young, G. M. (1982). Early Proterozoic climates and plate motions inferred from major element chemistry of lutites. *Nature*, 299(5885), 715–717. <https://doi.org/10.1038/299715a0>
- Pieters, C. M. (1983). Strength of mineral absorption features in the transmitted component of near-infrared reflected light: First results from RELAB. *Journal of Geophysical Research*, 88(B11), 9534–9544. <https://doi.org/10.1029/jb088ib11p09534>
- Potter-McIntyre, S. L., Chan, M. A., & McPherson, B. J. (2014). Concretion formation in volcanoclastic host rocks: Evaluating the role of organics, mineralogy, and geochemistry on early diagenesis. Early diagenesis and concretion formation in volcanoclastic host rock. *Journal of Sedimentary Research*, 84(10), 875–892. <https://doi.org/10.2110/jsr.2014.58>
- Rampe, E. B., Blake, D. F., Bristow, T. F., Ming, D. W., Vaniman, D. T., Morris, R. V., et al. (2020). Mineralogy and geochemistry of sedimentary rocks and eolian sediments in Gale crater, Mars: A review after six Earth years of exploration with Curiosity. *Geochemistry*, 80(2), 125605. <https://doi.org/10.1016/j.chemer.2020.125605>
- Rampe, E. B., Bristow, T. F., Blake, D. F., Vaniman, D. T., Chipera, S. J., Downs, R. T., et al. (2022). Mineralogical trends over the clay-sulfate transition in Gale crater from the Mars science Laboratory CheMin instrument, 53rd Lunar and Planetary science conference. 2678.
- Rampe, E. B., Ming, D. W., Blake, D. F., Bristow, T. F., Chipera, S. J., Grotzinger, J. P., et al. (2017). Mineralogy of an ancient lacustrine mudstone succession from the Murray formation, Gale crater, Mars. *Earth and Planetary Science Letters*, 471, 172–185. <https://doi.org/10.1016/j.epsl.2017.04.021>
- Rapin, W., Dromart, G., Rubin, D., Deit, L. L., Mangold, N., Edgar, L. A., et al. (2021). Alternating wet and dry depositional environments recorded in the stratigraphy of Mount Sharp at Gale crater, Mars. *Geology*, 49(7), 842–846. <https://doi.org/10.1130/g48519.1>
- Rapin, W., Ehlmann, B. L., Dromart, G., Schieber, J., Thomas, N. H., Fischer, W. W., et al. (2019). An interval of high salinity in ancient Gale crater lake on Mars. *Nature Geoscience*, 12(11), 889–895. <https://doi.org/10.1038/s41561-019-0458-8>
- Rapin, W., Meslin, P.-Y., Maurice, S., Vaniman, D., Nachon, M., Mangold, N., et al. (2016). Hydration state of calcium sulfates in Gale crater, Mars: Identification of bassanite veins. *Earth and Planetary Science Letters*, 452, 197–205. <https://doi.org/10.1016/j.epsl.2016.07.045>
- Rice, M., Seeger, C., Bell, J., Calef, F., Clair, M., Eng, A., et al. (2022). Spectral diversity of rocks and soils in Mastcam observations along the Curiosity rover's traverse in Gale crater, Mars. *Earth and Space Science Open Archive*, 73. <https://doi.org/10.1002/essoar.10510632.1>
- Rivera-Hernández, F., Sumner, D. Y., Mangold, N., Banham, S. G., Edgett, K. S., Fedo, C. M., et al. (2020). Grain size variations in the Murray formation: Stratigraphic evidence for changing depositional environments in Gale crater, Mars. *Journal of Geophysical Research: Planets*, 125(2). <https://doi.org/10.1029/2019je006230>
- Rudolph, A., Horgan, B., Johnson, J. R., Bennett, K., Haber, J., Bell, J., III, et al. (2022). The distribution of clay minerals and their impact on diagenesis in Glen Torridon, Gale crater, Mars. *JGR: Planets*. <https://doi.org/10.1029/2021JE007098>
- Scheinost, A. C., Chavernas, A., Barrón, V., & Torrent, J. (1998). Use and limitations of second-derivative diffuse reflectance spectroscopy in the visible to near-infrared range to identify and quantify Fe oxide minerals in soils. *Clays and Clay Minerals*, 46(5), 528–536. <https://doi.org/10.1346/ccmn.1998.0460506>
- Sherman, D. M., & Waite, T. D. (1985). Electronic spectra of Fe₃₊ oxides and oxide hydroxides in the near IR and near UV. *American Mineralogist*, 70, 1262–1269.
- Siebach, K. L., Fedo, C. M., Edgar, L. E., Edgett, K., Grotzinger, J. P., Fraeman, A. A., et al. (2019). *Overview of Gale crater stratigraphy and sedimentology from 6 years of roving with Mars science laboratory*, 50th Lunar and Planetary Science Conference. 1479.
- Singer, A. (1980). The paleoclimatic interpretation of clay minerals in soils and weathering profiles. *Earth-Science Reviews*, 15(4), 303–326. [https://doi.org/10.1016/0012-8252\(80\)90113-0](https://doi.org/10.1016/0012-8252(80)90113-0)
- Smith, R. J., McLennan, S. M., Achilles, C. N., Dehouck, E., Horgan, B. H. N., Mangold, N., et al. (2021). X-Ray amorphous components in sedimentary rocks of Gale crater, Mars: Evidence for ancient formation and long-lived aqueous activity. *Journal of Geophysical Research: Planets*, 126(3). <https://doi.org/10.1029/2020je006782>
- Stack, K. M., Grotzinger, J. P., Kah, L. C., Schmidt, M. E., Mangold, N., Edgett, K. S., et al. (2014). Diagenetic origin of nodules in the sheepbed member, Yellowknife Bay formation, Gale crater, Mars: Diagenetic nodules in Gale crater. *Journal of Geophysical Research: Planets*, 119(7), 1637–1664. <https://doi.org/10.1002/2014je004617>
- Starr, M. S., Rice, M. S., Hughes, C. M., Seeger, C. H., Bell, J. F., III, & Wellington, D. F. (2019). Methodology for the creation and analysis of a comprehensive Mastcam multispectral database of Curiosity's traverse. *LPI Contrib. No.*, 2132, 3087.
- Stein, N., Grotzinger, J. P., Schieber, J., Mangold, N., Hallet, B., Newsom, H., et al. (2018). Desiccation cracks provide evidence of lake drying on Mars, Sutton Island member, Murray formation, Gale crater. *Geology*, 46(6), 515–518. <https://doi.org/10.1130/g40005.1>
- Summons, R. E., Amend, J. P., Bish, D., Buick, R., Cody, G. D., Marais, D. J. D., et al. (2011). Preservation of Martian organic and environmental records: Final report of the Mars biosignature working group. *Astrobiology*, 11(2), 157–181. <https://doi.org/10.1089/ast.2010.0506>
- Sun, V. Z., Stack, K. M., Kah, L. C., Thompson, L., Fischer, W., Williams, A. J., et al. (2019). Late-stage diagenetic concretions in the Murray formation, Gale crater, Mars. *Icarus*, 321, 866–890. <https://doi.org/10.1016/j.icarus.2018.12.030>
- Thompson, L. M., Berger, J. A., Spray, J. G., Fraeman, A. A., McCraig, M. A., O'Connell-Cooper, C. D., et al. (2020). APXS-derived compositional characteristics of Vera Rubin Ridge and Murray formation, Gale crater, Mars: Geochemical implications for the origin of the ridge. *Journal of Geophysical Research: Planets*, 125(10). <https://doi.org/10.1029/2019JE006319>
- Velde, B. (1995). Origin and mineralogy of clays. <https://doi.org/10.1007/978-3-662-12648-6>
- Wattel-Koekkoek, E. J. W., & Buurman, P. (2004). Mean residence time of Kaolinite and SMECTITE-Bound organic matter in Mozambiquan soils. *Soil Science Society of America Journal*, 68(1), 154–161. <https://doi.org/10.2136/sssaj2004.1540>
- Wellington, D. F., Bell, J. F., Johnson, J. R., Kinch, K. M., Rice, M. S., Godber, A., et al. (2017). Visible to near-infrared MSL/MASTCAM multispectral imaging: Initial results from select high-interest science targets within Gale Crater, Mars. *American Mineralogist*, 102(6), 1202–1217. <https://doi.org/10.2138/am-2017-5760ccby>

- Wiens, R. (2013). MSL chemcam laser induced breakdown spectrometer EDR V1.0 [Dataset]. NASA Planetary Data System. Retrieved from <https://pds.nasa.gov/ds-view/pds/viewProfile.jsp?dsid=MSL-M-CHEMCAM-LIBS-2-EDR-V1.0>
- Wiens, R. C., Maurice, S., Barraclough, B., Saccoccio, M., Barkley, W. C., Bell, J. F., et al. (2012). The ChemCam instrument suite on the Mars Science Laboratory (MSL) rover: Body unit and combined system Tests. *Space Science Reviews*, 170(1–4), 167–227. <https://doi.org/10.1007/s11214-012-9902-4>
- Worden, R. H., & Morad, S. (1999). Clay mineral cements in sandstones. <https://doi.org/10.1002/9781444304336>
- Yen, A. S., Ming, D. W., Vaniman, D. T., Gellert, R., Blake, D. F., Morris, R. V., et al. (2017). Multiple stages of aqueous alteration along fractures in mudstone and sandstone strata in Gale Crater, Mars. *Earth and Planetary Science Letters*, 471, 186–198. <https://doi.org/10.1016/j.epsl.2017.04.033>